Nanoenergy Communications
https://www.sciltp.com/journals/nc

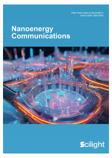

Review

Flexible Triboelectric Nanogenerators for Ocean Current Energy Harvesting: Mechanisms, Materials, Challenges, and Future Directions

Kefan Yang [1], Yi Zhang [1], Shengqing Zeng [1], Keqi Yang [2], Yunsheng Ma [2], Yixuan Zeng [1] and Dapeng Zhang [1,3,*]

[1] Ship and Maritime College, Guangdong Ocean University, Zhanjiang 524005, China
[2] School of Electronics and Information Engineering, Guangdong Ocean University, Zhanjiang 524088, China
[3] Guangdong Provincial Key Laboratory of Intelligent Equipment for South China Sea Marine Ranching, Guangdong Ocean University, Zhanjiang 524088, China
* Correspondence: zhangdapeng@gdou.edu.cn

How To Cite: Yang, K.; Zhang, Y.; Zeng, S.; et al. Flexible Triboelectric Nanogenerators for Ocean Current Energy Harvesting: Mechanisms, Materials, Challenges, and Future Directions. *Nanoenergy Communications* **2026**, *1*(1), 4.

Received: 30 December 2025
Revised: 29 January 2026
Accepted: 7 February 2026
Published: 12 February 2026

Abstract: Marine environmental monitoring and other missions demand long-term power supply for equipment. Addressing the shortcomings of existing power supply methods, this paper focuses on flexible triboelectric nanogenerators (FOCE-TENG), a novel marine current energy harvesting technology, and reviews its latest research progress. This technology efficiently captures low-velocity marine current energy and is suitable for scenarios where traditional technologies struggle to operate. Drawing on interdisciplinary theories, the paper elucidates key aspects including flow-induced vibration mechanisms, power generation performance regulation, and testing systems. It demonstrates that optimizing structural design and materials can enhance efficiency and stability. While challenges remain, such as adapting to extreme environments, future technological advancements hold promise for engineering applications, enabling sustainable power supply for underwater equipment.

Keywords: triboelectric nanogenerator; flow-induced vibration power generation; energy harvesting; power supply mode

1. Introduction

The strategic importance of the oceans has been increasingly recognized, and as a result, maritime affairs have been elevated to an unprecedented level of strategic importance among nations. It is evident that tasks such as marine resource exploration, environmental monitoring, and maritime security require long-term observation capabilities, in addition to close-range, real-time, and continuous observation. Existing methods, such as satellites, ships and submarines, are inadequate in meeting these demands. Underwater wireless sensor networks [1–5] utilize acoustic waves as their transmission medium, forming intelligent network systems through distributed static and dynamic sensor nodes that collect, transmit, and fuse data. These networks are of paramount importance in the safeguarding of maritime rights and interests, the development of resources, the provision of disaster early warning systems, and national defense.

Presently, the utilization of underwater sensor nodes [6–10] predominantly depends on direct cable power supply, battery power, or solar-battery hybrid power systems. However, as observation cycles lengthen, node numbers increase, and deployment ranges expand, these powering methods reveal significant limitations: cables are susceptible to seawater corrosion and face installation constraints; batteries have limited capacity, incurred high replacement and maintenance costs, and posed risks of leakage and corrosion. As marine energy harvesting technologies, including wave, thermal and ocean current energy, continue to develop and mature, they offer significant potential as sustainable energy replenishment pathways for sensor nodes.

Research institutions worldwide continue to explore this field. For instance, Southeast University [11] proposed a direct-drive cylindrical wave energy converter capable of efficiently converting wave energy into electricity; The Guangzhou Institute of Energy Conversion, Chinese Academy of Sciences [12] developed a novel floating hydraulic energy conversion system to enhance efficiency; Michigan Technological University [13] designed an array-based wave energy converter enabling buoys to collect energy through oscillation while carrying equipment. Additionally, thermoelectric energy-driven monitoring platforms [14–16] have attracted attention from multiple institutions including China Shipbuilding Industry Corporation and the National University of Defense Technology. Compared to other renewable energy sources, ocean current energy offers advantages such as high energy flux density and stable output. However, existing impeller-based collection technologies [17–19] are primarily suited for high-power generation and are constrained by factors like flow velocity, corrosion, and direction. Therefore, there is an urgent need to develop new ocean current energy collection technologies suitable for underwater sensor nodes.

In recent years, triboelectric nanogenerators (TENGs) have emerged as a promising solution to these challenges. The TENG operates on the basis of the coupling effect of triboelectric charging and electrostatic induction, thereby converting weak mechanical energy from the environment into electrical energy. The advantages offered by this approach include high sensitivity to low-frequency excitation, flexible structural design, broad material selection, lightweight construction, and low cost. The device has been demonstrated to be especially well-suited for the harvesting of irregular, low-frequency mechanical energy, thereby opening up new possibilities for distributed power supply and self-powered sensor networks [20–24].

In order to effectively capture ocean fluid energy, it is essential that energy harvesting devices adapt to the dynamic changes in water currents. Consequently, the integration of flexible materials with triboelectric nanogenerators (TENG) to develop flexible ocean current energy TENG (FOCE-TENG) has emerged as an important research direction in this field (as shown in Figure 1). The TENG's flexible structure endows it with outstanding mechanical compliance, thereby enabling full dynamic coupling with the fluid through deformations such as bending, stretching, or twisting, thus maximizing kinetic energy capture from ocean currents [25–27]. A plethora of studies have hitherto explored various biomimetic structures, including those simulating fish fin flapping [28–30] and flag-like designs [31]. These studies have demonstrated the feasibility of such structures in initiating operation and generating electricity in low-velocity water currents.

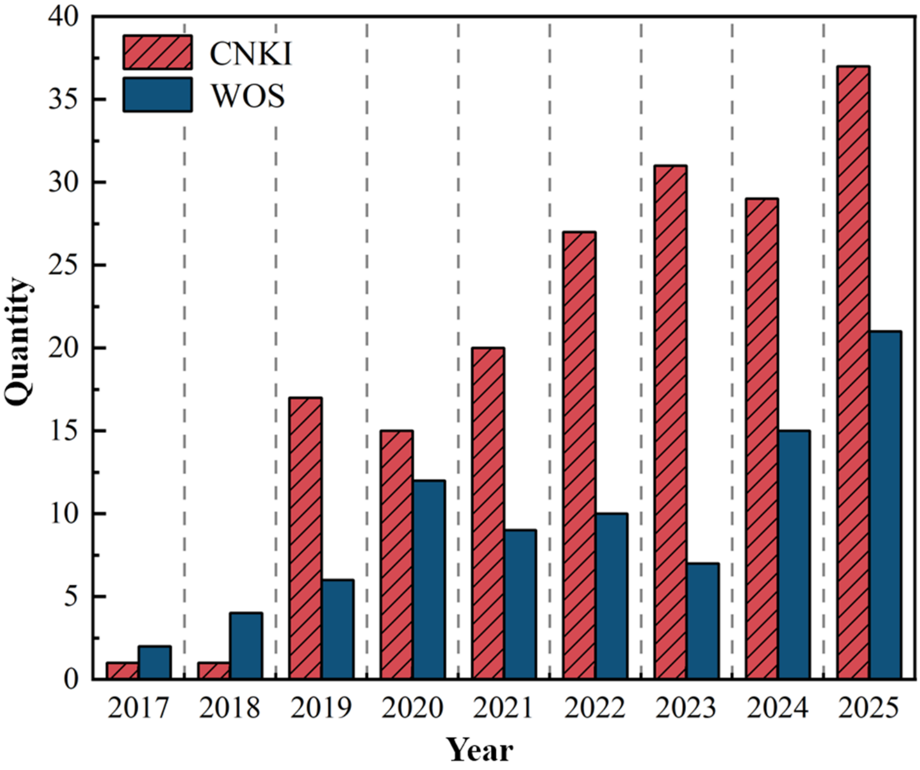

Figure 1. Publication output of FOCE-TENG literature on WOS and CNKI in recent years.

Although the FOCE-TENG demonstrates application potential in marine fluid energy harvesting, it still faces numerous challenges in advancing from laboratory-scale proof-of-concept to large-scale practical deployment. Taking the impeller-based device as an example, the Alstom marine current energy system [32] adopted by Tidal Generation Limited of the UK employs a fixed-bottom support structure, equipped with a self-driven impeller and variable-pitch blades. Its ideal operating flow velocity ranges from 2.57 to 3.6 m/s, whereas the flow velocity in most coastal areas is merely 0.5 to 1.5 m/s, which can hardly meet the operational requirements. The current velocity in the flow profile generally decreases sharply with increasing water depth, and complex variations in current direction further reduce the energy capture efficiency. In addition, electromagnetic generators relying on large magnets, metal coils and turbine structures require floating platforms or fixed seabed structures, resulting in high costs and complex installation, which restricts the large-scale deployment of impeller-based technologies.

Non-impeller marine tidal current energy harvesters are mainly designed for low-flow-velocity and low-power generation scenarios. For instance, Ocean University of China developed a low-velocity energy conversion device based on the principle of vortex-induced vibration [33]; Engineering Business of the United Kingdom created the "Stingray" device, which generates power through hydrofoil oscillation that drives a hydraulic system [34]; and Hiroshima University proposed a vibration-based power generation device utilizing flexible piezoelectric materials [35]. Nevertheless, such devices commonly suffer from issues including proneness to instability under high flow velocities and restricted energy conversion efficiency. Therefore, optimizing the energy capture and power absorption mechanisms, as well as improving energy utilization efficiency and reducing generation costs, still constitutes the core objective of this field.

This review systematically summarizes the latest research progress of flexible triboelectric nanogenerators in the field of marine fluid energy harvesting. Based on multidisciplinary theories such as fluid mechanics and materials science, it focuses on three core modules: flow-induced vibration mechanisms, power generation performance regulation, and system optimization and application. This review elaborates on the current achievements, analyzes the key issues, and prospects the development directions, aiming to provide a systematic reference for the in-depth research of FOCE-TENGs and offer forward-looking guidance for their realization of efficient and stable energy harvesting as well as the promotion of the practical application of blue energy.

2. Study on the Mechanism of Flow-Induced Vibration

FOCE-TENG, as an innovative solution for capturing low-speed ocean current energy, relies on the systematic integration of fluid mechanics, materials science, and triboelectric nanogenerator (TENG) technology to establish a complete theoretical chain from "environmental excitation to functional output" [36–39]. Within this framework, fluid mechanics not only provides periodic driving forces based on flow-induced vibration and vortex shedding but also deeply couples with device structural parameters through solid-liquid interface interaction mechanisms [37,40,41], fundamentally guiding design, optimization, and output behavior prediction [42–49]. Conversely, the physicochemical properties of material systems dictate device performance limits, environmental adaptability, and functional expansion potential, constituting core materials science challenges [50–53]. As a specialized branch of TENG technology, fluid-driven TENGs exhibit remarkable diversity in configuration, mechanisms, and applications [54–58], with their developmental trajectory fully embodying an integrated research paradigm spanning fundamental scientific principles to engineering practice [59–63].

An interdisciplinary theoretical framework has been established, confirming that flow-induced vibration is the core physical process by which flexible ocean current energy friction nanogenerators capture ocean current energy. The amplitude, frequency, and modes of this vibration directly determine the device's charge transfer efficiency and power output. Based on fluid dynamics principles, this chapter will delve into the microscopic mechanisms of flow-induced vibration. Through theoretical modeling and parameter optimization, this study quantitatively reveals the correlation between ocean current loads, structural parameters, and vibration responses. This research elucidates the intrinsic logic of fluid-structure interaction within the "ocean current-bulkhead-flexible structure" system, providing precise guidance for the structural optimization design of flexible ocean current energy triboelectric nanogenerators.

Modeling and Parameter Solving of Flow-Induced Vibration Theory

In the context of marine flow fields, the FOCE-TENG system necessitates the development of a theoretical model that accurately characterizes the dynamic response of flexible structures in complex ocean currents. This model is essential for the accurate prediction of flow-induced vibrations, which are critical for the effective operation of the system. This involves the quantification of the intrinsic relationship between ocean current loads and structural vibrations through multiphysics coupling equations, and the solution of key parameters such as amplitude, vibration frequency, and force-to-electricity conversion efficiency. This theoretical framework provides a foundation for the optimization of device performance and the development of marine engineering applications. Building upon the foundations of fluid-structure interaction theory and integrating triboelectric conversion mechanisms, extant research has established multiple models with theoretical underpinnings that are relevant to engineering applications. Through experimental validation and parameter sensitivity analysis, these studies have elucidated the regulatory patterns of key design parameters on device output performance.

Flow-induced vibration is the core physical process for FOCE-TENG to capture ocean current energy, and its amplitude, frequency, and mode directly determine charge transfer efficiency. The theoretical model of flow-induced vibration needs to comprehensively consider three core forces: ocean current viscous force, unsteady excitation force from vortex shedding, and elastic recovery force of flexible materials.

As shown in Figure 2, based on the research by Wang et al. [45], the mass ratio M^* (involving fluid and flaglet density, length, and thickness) and bending stiffness K_b (involving Young's modulus, Poisson's ratio, and structural dimensions) of the fluid-structure interaction system significantly influence the critical activation velocity of flexible ocean current energy harvesting triboelectric nanogenerators. For instance, by optimizing the parameters of the flexible ocean current energy harvesting triboelectric nanogenerator, the critical activation velocity can be reduced to 0.133 m/s, enabling energy harvesting in low-speed ocean currents.

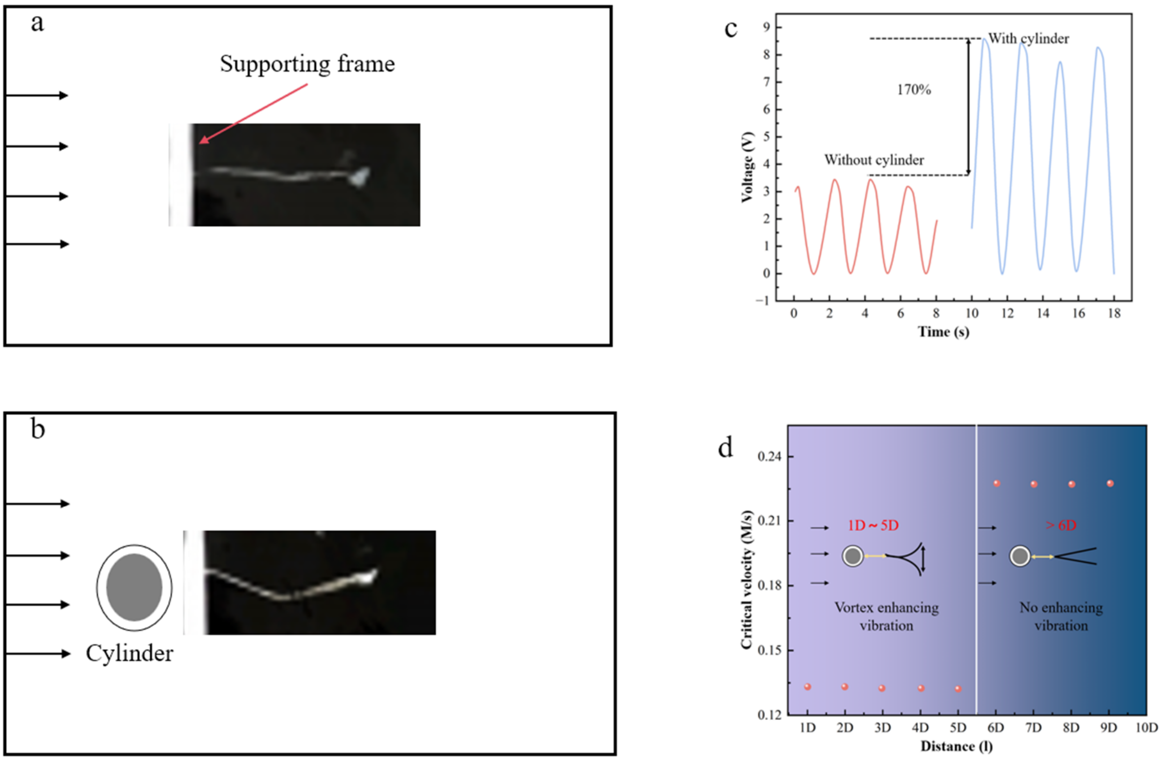

Figure 2. The vibration characteristics of the flag TENG: (**a**) vibration-free state; (**b**) vibration state caused by the vortex in the cylinder at a flow rate of 0.228 m per second; (**c**) Comparison of output voltage signals of Flag TENG; (**d**) The relationship between the critical speed and the distance between the flag TENG and the cylinder.

In the field of dynamic equation formulation, the vibration behavior of flexible structures is often simplified by modeling them as spring-damper-mass systems. Subsequently, a complete electromechanical coupling dynamics model is established by introducing friction-electric coupling terms. Taking the fully encapsulated FOCE-TENG device proposed by Zeng et al. [64] as an example, this structure can be modeled as a spring-damper-mass system undergoing lateral vibration. Building upon this theoretical framework, this study further elucidates the regulatory mechanisms of two structural inertia parameters—additional mass m and rotational radius r—on electrode contact separation efficiency. Figure 3 demonstrates that with a fixed rotation radius of 30 mm and an added mass of 3 g, the transferred charge quantity Q_{sc} increases by 18.9% compared to the case without added mass. This result confirms that structural inertia parameters exert a significant positive regulatory effect on force-to-electricity conversion efficiency.

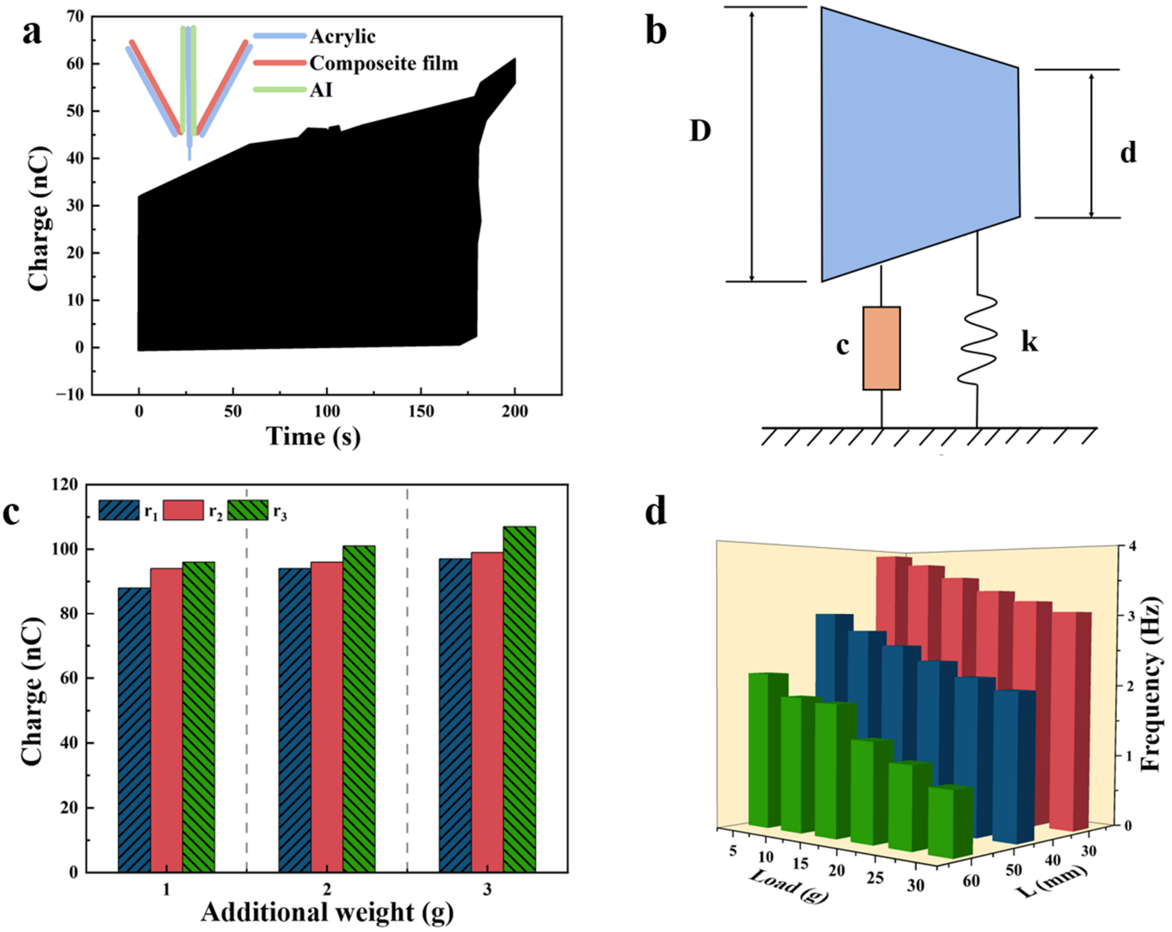

Figure 3. FIV-TENG configuration optimization: (**a**) The curve of the transfer charge of FIV-TENG varying with time under the flat plate electrode structure; (**b**) Schematic diagram of the physical model of the FIV-TENG oscillation system; (**c**) Comparison of the transferred charges of FIV-TENG under different additional masses and rotation radii; (**d**) Oscillation frequency distribution of FIV-TENG under different additional masses and cantilever beam lengths.

In the practical implementation of flow-induced vibration models, the precise determination of parameters and system optimization are critical steps. The prevailing approach in contemporary research utilizes a multifaceted strategy that integrates theoretical derivation, numerical simulation, and experimental validation to ascertain the optimization ranges for diverse core parameters [65]. It is imperative to emphasize that, among these factors, the optimization of structural parameters is of particular significance. For instance, in their study on trapezoidal vibrators for FOCE-TENG, Zhu et al. [66] first established a theoretical model describing fluid-induced forces based on the quasi-steady assumption:

$$F_{air} = \frac{1}{2}\rho U^2 D \sum_{i=1}^{n} \phi_1 \left(\frac{\dot{y}}{U}\right)^i \tag{1}$$

Subsequently, their research employed the Krylov-Bogoliubov approximate analytical method to treat the system’s dynamic equations, thereby establishing the relationship between the normalized amplitude and the cross-sectional geometry, flow velocity, and mass damping parameter. Based on this foundation, an analytical expression for the normalized vibration amplitude was further derived. By substituting experimental parameters into this equation as described in [66], calculations revealed that under conditions of angle of attack $\alpha = 0°$, base length ratio $\frac{d}{D} = 0$ (i.e., triangular oscillator), and reduced flow velocity $U_r = 10$, the maximum normalized amplitude reached $\frac{A_{Yrms}}{D} = 0.703$. This corresponds to an output power of 24.056 mW, representing approximately a threefold increase compared to a square-section oscillator. This result strongly confirms the significant influence of blunt-body cross-sectional geometry on flow-induced vibration response, thereby providing clear theoretical basis for optimizing oscillator cross-sectional geometry.

Additionally, flow field parameters constitute critical influencing factors. Zhang et al. [43] investigated vortex-induced vibration-type nanogenerators by employing fast Fourier transform analysis to examine structural vibration spectra at varying flow velocities. Integrating theoretical formulas, they elucidated the energy conversion mechanism within the frequency locking range. On one hand, the frequency prediction value calculated based on classical vortex shedding frequency theory was 13.8 Hz; on the other hand, the experimentally measured primary vibration frequency of the cylinder was 14.3 Hz, demonstrating high consistency between the two. This result jointly confirms from both theoretical and experimental perspectives that structural vibration synchronizes with the vortex shedding frequency within the locked-frequency range, thereby providing a physical basis for the efficient conversion of flow field energy into mechanical vibration.

Finally, the regulatory role of force-electric coupling parameters in the system's dynamic behavior is also crucial. As revealed by Abdelkefi et al. [67] through linear eigenvalue analysis, the load resistance R can effectively modulate the system's overall natural frequency. This conclusion stems from the analysis of the system state matrix and its characteristic equation: By establishing state variables encompassing column displacement, velocity, and output voltage, the motion equations can be transformed into a matrix form within the state space. Here, the electrical term reflecting the rate of change of output voltage is directly related to the load resistance. It influences the mechanical vibration of the column through feedback via the electromechanical coupling coefficient, thereby globally altering the system's dynamic characteristics, including its natural frequency. Solving the characteristic equation of this state matrix further reveals that the system's characteristic roots—particularly the imaginary part of the complex conjugate roots determining the global frequency—strongly depend on the load resistance value. This directly confirms the significant regulatory effect of resistance on the system's natural frequency.

When changes in the load resistance alter the system's natural frequency, the synchronization range between this frequency and the vortex shedding excitation frequency in the flow field also shifts. The underlying physical mechanism is that the vortex shedding frequency increases with rising flow velocity. Therefore, when increased resistance raises the system's natural frequency, a higher flow velocity is required to match the vortex shedding frequency with the new natural frequency, thereby entering the high-amplitude synchronous locking range. Concurrently, the system exhibits typical nonlinear hardening characteristics. This stems from the cubic nonlinear term in the lift coefficient model, causing the resonance peak to shift toward higher frequencies as flow velocity increases. Furthermore, under high-load resistance conditions (as shown in Figure 4), the system's initial conditions significantly influence steady-state power output: the power-velocity curve exhibits pronounced hysteresis, with output power differing by up to an order of magnitude at the same flow velocity due to varying initial conditions. In contrast, under low- or medium-resistance conditions, the influence of initial conditions is negligible.

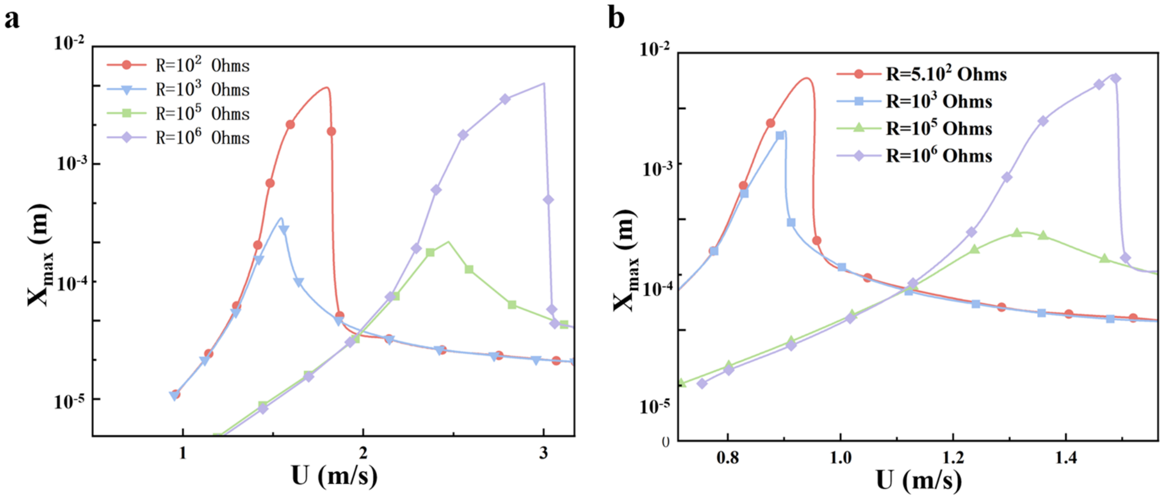

Figure 4. Lateral displacement of (**a**) the first configuration and (**b**) the second configuration under different load resistance values. Data sourced from [67].

Based on the above complex nonlinear and parameter-dependent characteristics; in order to maximize the energy harvesting efficiency, it is necessary to determine the optimal load matching relationship through numerical simulation covering multiple working conditions. The results of their system analysis under short-circuit and open-circuit configurations further prove [67] that only through extensive parameter simulation and comprehensive consideration of different combinations of load resistance and inflow velocity can the load parameters that can maximize energy harvesting performance be ultimately determined.

3. Research on Power Generation Performance Regulation of FOCE-TENG

The analysis of the flow-induced vibration mechanism elucidates the energy input pathway for FOCE-TENG. In order to efficiently convert vibrational kinetic energy into stable electrical energy, it is also necessary to regulate performance at the levels of core device components and system integration. The "contact-separation-charge transfer" process is influenced by parameters such as vibration amplitude and frequency, which in turn impact power generation output. The efficiency of this process is contingent upon the conductivity of flexible electrodes, the charge storage capacity of dielectric materials, the contact characteristics of surface micro/nano structures, and the synergistic effects of multi-unit networking. This chapter systematically delineates methodologies for the regulation of power generation performance through the optimization of core components and the design of network configuration. It establishes a quantitative mapping relationship between "vibration parameters—charge transfer—electrical energy output".

3.1. FOCE-TENG Power Generation Theoretical Model

The fundamental principle underlying FOCE-TENG's power generation theory resides in the coupling mechanism between flow-induced vibration and triboelectric charge transfer. The model's construction must encompass both fluid dynamics principles and the fundamental nature of TENG charge transfer. This will enable quantitative prediction of power generation performance based on vibration parameters.

3.1.1. Core Theoretical Framework

The power generation theory of FOCE-TENG is based on the charge transfer mechanism of contact-dissociation-type independent-layer triboelectric nanogenerators, combined with the dynamics of flow-induced vibration, forming a closed-loop coupled model. Its driving mechanism originates from flow-induced vibration, whose characteristics are dominated by fluid-structure interaction. As shown in Figure 5, the fluid-solid mass ratio model and the dimensionless bending stiffness model established by Wang et al. [45] demonstrate that the vibration amplitude and frequency dynamically evolve with flow velocity, structural dimensions, and material properties. Meanwhile, the effective contact area of the TENG and its variation frequency are proportional to the contact separation period frequency, thereby directly regulating its power generation performance through the charge transfer equation.

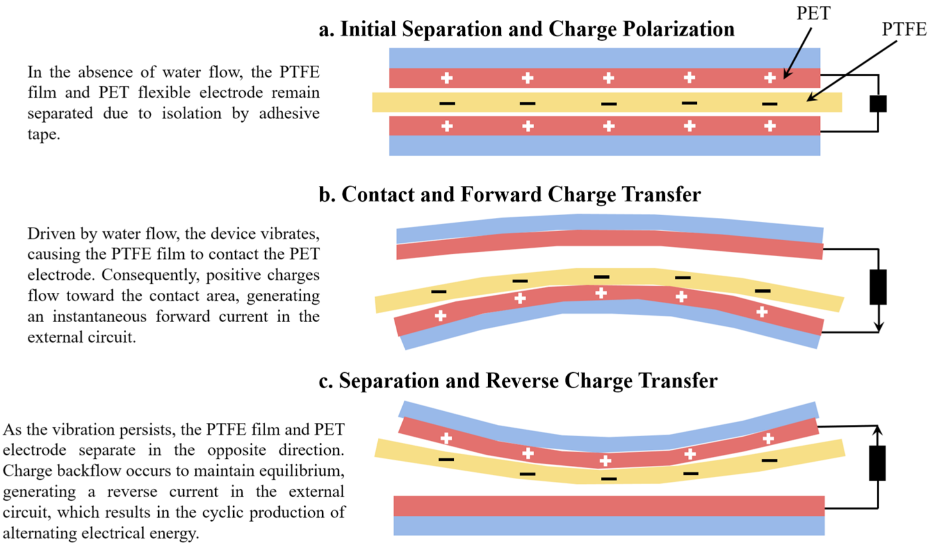

a. Initial Separation and Charge Polarization

In the absence of water flow, the PTFE film and PET flexible electrode remain separated due to isolation by adhesive tape.

b. Contact and Forward Charge Transfer

Driven by water flow, the device vibrates, causing the PTFE film to contact the PET electrode. Consequently, positive charges flow toward the contact area, generating an instantaneous forward current in the external circuit.

c. Separation and Reverse Charge Transfer

As the vibration persists, the PTFE film and PET electrode separate in the opposite direction. Charge backflow occurs to maintain equilibrium, generating a reverse current in the external circuit, which results in the cyclic production of alternating electrical energy.

Figure 5. The schematic diagram of the working principle can visually verify the closed-loop process of "vibration—contact separation—charge transfer".

3.1.2. Quantitative Relationships and Experimental Verification

In light of the theoretical analyses, models, and empirical cases previously discussed, the following core conclusion is reached: the charge transfer in FOCE-TENG can be represented by the following simplified model:

$$Q \propto A \cdot f \cdot \sigma \tag{2}$$

The physical effects of each parameter and their experimental basis are as follows:

(1) Effect of amplitude (*A*)

The amplitude is jointly determined by the range of relative displacement within the friction layer and the effective contact area. Liu et al. [68] demonstrated through circulating water tank experiments that when the simulated ocean current velocity increased from 0.133 m/s to 0.511 m/s, the amplitude of the flexible TENG rose from approximately 3 mm to 12 mm. The increase in effective contact area enhanced charge transfer by about threefold, consistent with the $Q \propto A$ relationship. Subsequent research by Wang et al. [45] further confirmed that under supercritical flow conditions, doubling the amplitude can increase the output voltage (positively correlated with *Q*) by approximately 80–100%, highlighting the significant contribution of amplitude to charge transfer.

(2) Effect of frequency (*f*)

The vibration frequency characterizes the number of contact-separation events per unit time, directly influencing the charge transfer rate. As shown in Figure 6, Liu et al.'s wave simulation experiments [68] demonstrated that when the amplitude was maintained at 8 mm, increasing the frequency from 0.25 Hz to 1.25 Hz elevated the output current from 0.5 μA to 2.6 μA, with the transferred charge increasing approximately 4.2-fold, consistent with the $Q \propto f$ relationship.As shown in Figure 7, further research by Wang et al. [45] indicates that flow-induced vibration frequency is proportional to flow velocity. Higher frequencies reduce contact-separation cycles, thereby accelerating charge transfer. This conclusion is also supported by indirect experimental evidence.

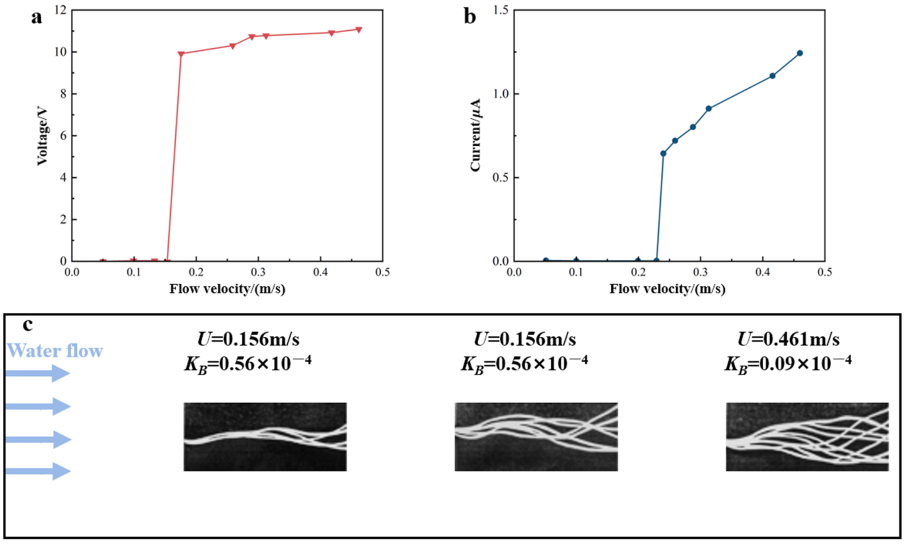

Figure 6. Flag-type TENG (**a**) Output voltage versus flow velocity; (**b**) Output current versus flow velocity data; (**c**) Comparison of UF-TENG oscillation amplitude at different flow velocities.

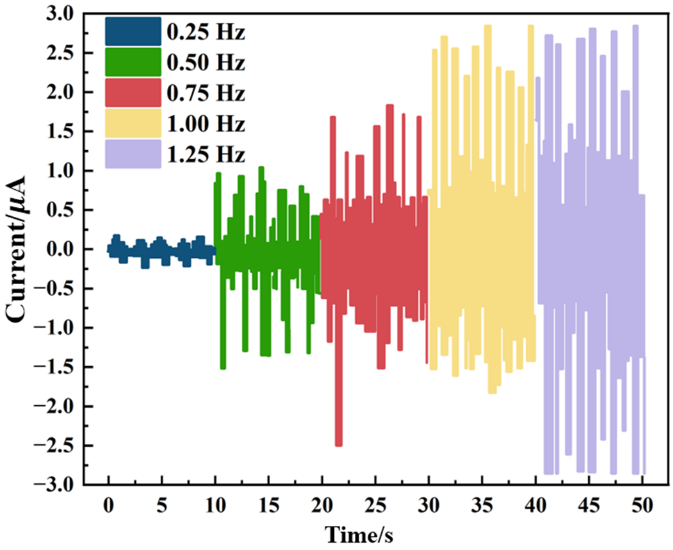

Figure 7. F-TENG output current under different frequency wave conditions.

(3) Effect of surface charge density (σ)

Surface charge density is determined by the intrinsic properties of friction materials and their surface microstructure, serving as a key parameter governing device performance. Zhang et al. [20] constructed composite nanostructures by doping gold nanoparticles into PTFE films, achieving a 1.7–7.5-fold increase in σ. They observed a corresponding enhancement in charge transfer capability (see Figure 8), directly validating the $Q \propto \sigma$ relationship and demonstrating that σ is the fundamental factor determining charge transfer capacity.

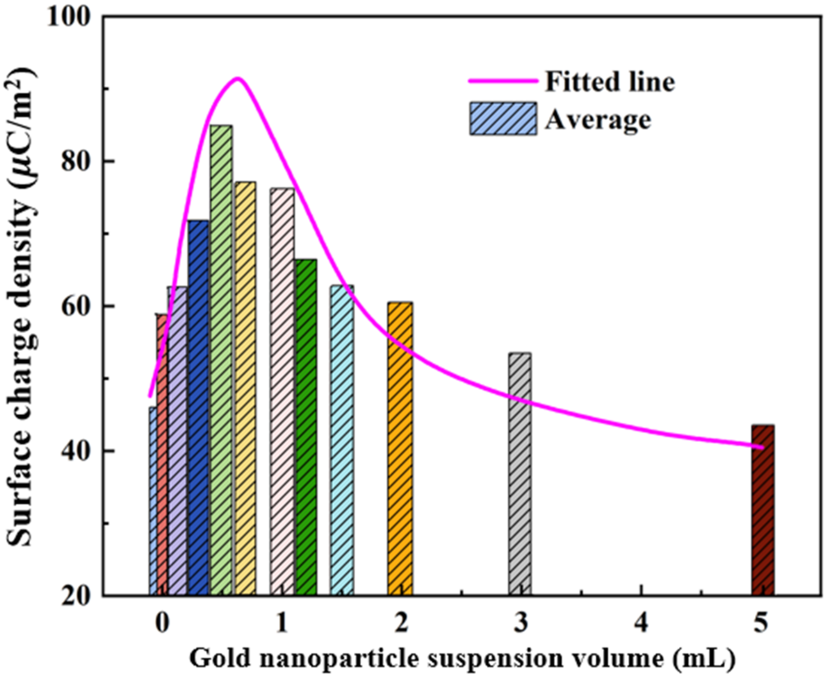

Figure 8. Relationship curve between nano-gold particle doping concentration and surface charge density. Data from [20].

3.1.3. Engineering Application and Validation of Theoretical Models

The FOCE-TENG power generation theoretical model provides a systematic theoretical basis for the engineering design, performance optimization, and practical application of ocean tidal energy harvesting devices by quantifying the regulatory mechanism of charge transfer quantity Q through vibration parameters (amplitude A, frequency f) and material parameters (surface charge density σ). The fundamental principles of this model have been thoroughly validated by multiple literature studies and empirical evidence.

The model reveals the regulatory patterns of key parameters on power generation performance, providing precise guidance for enhancing engineering performance. Regarding amplitude regulation, Liu et al. [68] discovered through circulating water tank experiments that increasing the amplitude from 5 mm to 10 mm (while maintaining a frequency of 1 Hz) expands the effective contact area of the friction layer, doubling the charge transfer rate. This phenomenon remains stable within a flow velocity range of 0.133–0.511 m/s. Wang et al. [45] further confirmed in UF-TENG experiments that doubling the amplitude beyond the critical flow velocity increases the output voltage (positively correlated with Q) by 80–100%, providing experimental evidence for enhancing amplitude at low flow rates through structural optimization.

Regarding frequency regulation, the kinetic analysis by Wang et al. [45] and the wave simulation experiments by Liu et al. [68] jointly demonstrate that increasing the frequency from 0.5 Hz to 2 Hz (with amplitude fixed at 8 mm) triples the number of contact-separation cycles per unit time, correspondingly boosting charge transfer by approximately threefold. The characteristic that flow-induced vibration frequency is proportional to flow velocity provides theoretical support for achieving frequency optimization through flow velocity matching, enabling FOCE-TENG to maintain efficient charge transfer across a wide range of flow velocities.

In the optimization of material parameters, Zhang et al. [20] employed surface patterning and nanocomposite modification techniques to increase the surface charge density σ of friction materials by 1.7–7.5 times, thereby significantly enhancing charge transfer. This result validates the fundamental relationship "$Q \propto \sigma$" in the model, providing a basis for engineering material selection and surface treatment.

The model elucidates the regulatory mechanism of structural parameters on critical activation flow velocity by introducing submodels such as the fluid-solid mass ratio (Equation (2)) and the dimensionless bending stiffness (Equation (3)), providing a design paradigm for ultra-low flow velocity energy harvesting. Experiments by Wang et al. [45] demonstrate that by adjusting the aspect ratio and bending stiffness, the critical activation velocity of UF-TENG devices can be reduced to 0.133 m/s. This enables effective capture of extremely low-speed tidal currents, overcoming the bottleneck of insufficient adaptability in low-velocity marine environments faced by traditional electromagnetic and piezoelectric generators.

Regarding multi-unit integration, the parallel integration strategy proposed by Wang et al. [45] demonstrates that output power increases linearly with the number of units ($P_N = N \cdot P_1$). Experiments confirm that a six-unit parallel UF-TENG achieves a peak power of 52.3 μW at a flow velocity of 0.461 m/s, providing both theoretical and experimental foundations for arrayed high-power ocean tidal energy harvesting systems.

The practicality of this model has been validated in multiple marine engineering scenarios. In distributed marine sensing power supply, Liu et al. [68] designed and developed a flexible TENG device based on the model. It operates stably under tidal currents of 0.133–0.511 m/s and wave environments of 0.25–1.25 Hz, with a maximum output voltage of 24.8 V and with a maximum output current of 2.6 μA. The parallel output power of multiple units reached 79.023 μW, sufficient to meet the in-situ power supply requirements of low-power devices such as temperature-salinity-depth sensors and underwater thermometers. For ultra-low-speed flow energy harvesting, Wang et al. [45] developed a model-optimized UF-TENG device with a critical start-up velocity as low as 0.133 m/s. It demonstrated excellent performance in both recirculating tank experiments and simulated real ocean environments, showcasing its application potential for energy harvesting in low-velocity zones such as deep-sea and nearshore areas.

The current model still has certain limitations, primarily manifested in insufficient consideration of the impact of deep-sea high-pressure environments on charge transfer processes. High pressure may alter the dielectric properties of the friction layer, exacerbating charge dissipation and limiting the model's direct applicability in deep-sea engineering. It is recommended that future engineering improvements incorporate deep-sea environmental characteristics, investigate the influence of high pressure on surface charge density and contact separation efficiency, and enhance the model's pressure adaptability. Concurrently, the physical-information artificial intelligence inverse design method proposed by Jiao et al. [69] can be adopted. Figure 9 illustrates the integrated architecture of the Internet of Things (IoT), artificial intelligence (AI), and flexible ocean current energy triboelectric nanogenerators (FOCE-TENG). This architecture harnesses ocean current energy through FOCE-TENG arrays, employs IoT modules for data sensing and transmission, and leverages AI engines for performance optimization, achieving intelligent coordination between marine energy harvesting and environmental adaptation. This approach integrates multi-field coupled simulations with experimental data to enhance the model's predictive accuracy and adaptability in complex marine environments. Consequently, it will facilitate the expansion of FOCE-TENG applications from nearshore shallow-water settings to large-scale deep-sea ocean energy harvesting projects.

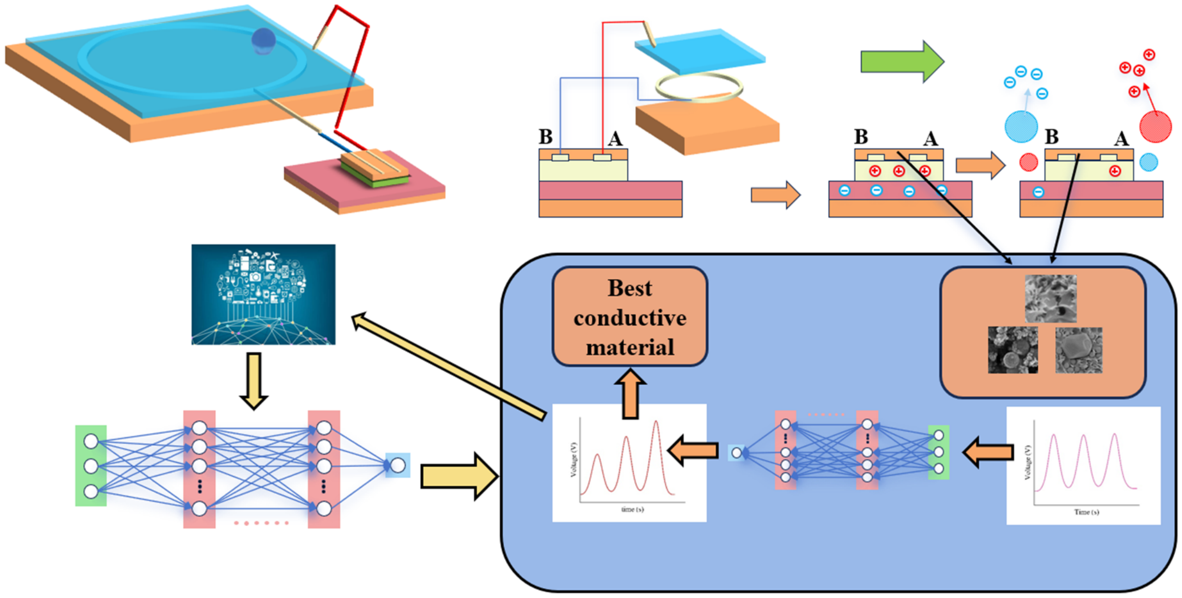

Figure 9. Integration of IoT, AI, and FOCE-TENG.

3.2. Study on the Impact of Core Components on Power Generation Performance

The theoretical model of FOCE-TENG power generation has quantified the influence of key parameters such as amplitude, frequency, and surface charge density on charge transfer, thereby providing a theoretical basis for performance regulation. The optimization of these parameters ultimately requires structural design and material modification of core components, namely flexible electrodes as charge conduction carriers, dielectric materials as charge generation and storage cores, and surface micro/nano structures as key elements for contact efficiency optimization. Collectively, these elements constitute the core regulatory mechanisms that govern the performance of power generation (as shown in Table 1). The subsequent section will analyze the optimization pathways and performance impact mechanisms of each component, thereby providing technical support for the engineering implementation of the theoretical model.

Table 1. Optimization strategy for FOCE-TENG core components.

Core Components	Research Content and Technical Pathways	Key Indicators
Flexible electrodes	Comparison of multi-process fabrication and surface treatment effects	Charge transfer amount, output voltage/current
Dielectric materials	Multi-material friction performance comparison and charge measurement	Electrification efficiency, charge transfer stability
Surface micro-nano structure	Microstructure construction, characterization, and contact mechanism analysis	Contact area utilization, performance improvement margin

3.2.1. Flexible Electrodes

As the core component of FOCE-TENG, the material properties of flexible electrodes—including conductivity, flexibility, mechanical stability, and environmental adaptability—directly determine the device's energy conversion efficiency, durability, and application potential in complex marine environments. Conventional metal electrodes demonstrate deficiencies in their capacity to adapt to the low-frequency fluctuations of ocean currents and long-term immersion conditions. These limitations are attributed to factors such as susceptibility to corrosion, inadequate flexibility, and substantial mass. Conversely, innovative flexible electrodes, including graphene-based and gel-based electrodes, have emerged as pivotal advancements for enhancing FOCE-TENG power generation performance through structural design and performance optimization [70]. This paper systematically analyses the impact of flexible electrodes on FOCE-TENG power generation performance across three dimensions: electrode material types, performance enhancement mechanisms, and marine environmental adaptability. These findings are based on recent research results.

Firstly, the flexible electrode materials commonly used in FOCE-TENG primarily include two categories: graphene-based composites and gel-based conductive materials. As shown in Table 2, through different structural designs, these materials meet the performance requirements for ocean current energy harvesting.

Table 2. Comparison of two flexible electrodes.

Performance Dimension	Graphene-Based Electrode	Gel-Based Electrode
Conductivity	High	Moderate
Flexibility	Flexible, low tensile strain	Highly stretchable, self-healing
Environmental Adaptability	Resistant to seawater corrosion, but not to low temperatures	Wide temperature range operation, resistant to biofouling
Cost	High	Low

As demonstrated in Figure 10, Xie et al. [70] utilized graphene and its derivatives—including graphene quantum dots (GQDs), graphene nanosheets (GNSs), reduced graphene oxide (rGO), laser-induced graphene (LIG), and chemical vapor deposition (CVD) graphene—as core materials, employing top-down or bottom-up fabrication processes. These electrodes demonstrate ultra-high conductivity, excellent mechanical flexibility, good corrosion resistance, and high light transmittance (approximately 97% for monolayer graphene), enabling them to withstand repeated deformation driven by ocean currents and prolonged immersion in seawater environments [71].

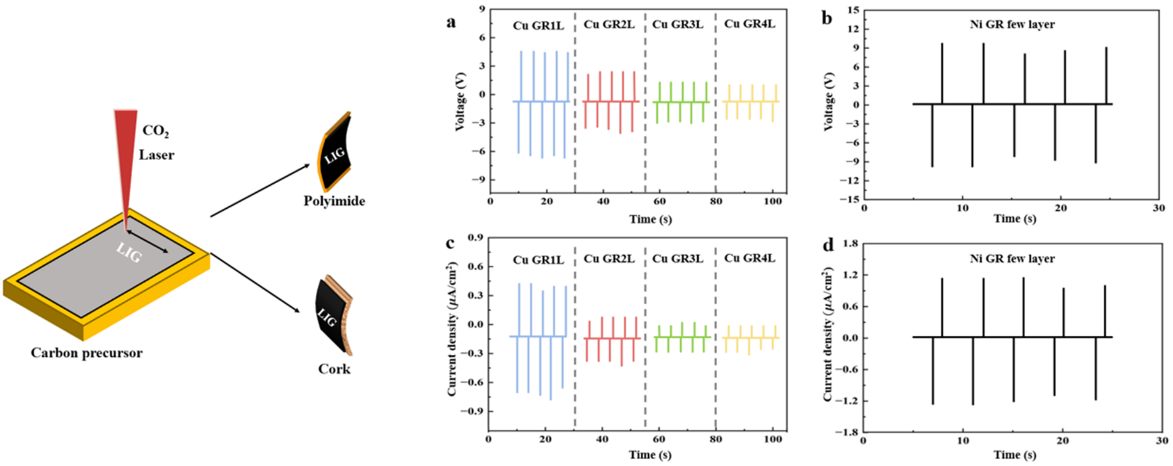

Figure 10. Graphene electrode TENG: (**a**) Output voltage versus current for layer-by-layer stacked graphene electrode TENG; (**b**) Output voltage versus current for multilayer graphene electrode TENG; (**c**) Output voltage versus current for layer-by-layer stacked graphene electrode TENG; (**d**) Output voltage versus current for multilayer stacked graphene electrode TENG. Data from [70].

As shown in Table 3, the second major category comprises gel-based flexible electrodes, primarily categorized into hydrogel electrodes, organic gel electrodes, and aerogel electrodes. Their core principle involves constructing a three-dimensional crosslinked network and loading conductive media to achieve the integration of flexibility and conductivity. Lu et al. [72] accomplished integrated conductivity and flexibility by constructing a three-dimensional network structure loaded with conductive media. The incorporation of MXene, CNT, and other materials into hydrogel electrodes has been demonstrated to enhance conductivity. The replacement of solvent in organic gels has been shown to enable operation at temperatures as low as −75 °C, thereby overcoming the issue of low-temperature freezing. The utilisation of high porosity and low density in aerogels has been demonstrated to optimise contact separation efficiency under ocean currents. These electrodes demonstrate biocompatibility, self-healing capabilities, and excellent adaptability to extreme environments, withstanding impacts from ocean currents and temperature fluctuations.

Table 3. Performance enhancement mechanisms and core performance characteristics of gel-based electrodes.

Gel Electrode Types	Conductive Medium	Key Performance Indicators	Marine Environmental Adaptability
MXene/Hydrogel	MXene Nanoplatelets	High conductivity; High tensile strength; Dual conductive pathways	Resistant to salt spray corrosion; Strong self-healing capability
CNT/Organic Gel	Carbon nanotube	Wide temperature range adaptation; Conductive stability	Resistant to low-temperature freezing; Resistant to organic solvent immersion
Graphene/Aerogel	Graphene nanosheets	Low density, high porosity; high charge accumulation	Lightweight and buoyant; Resistant to water current impact

Secondly, flexible electrodes enhance the energy conversion efficiency of FOCE-TENG by optimizing charge transport, interfacial contact, and mechanical adaptability.

In terms of charge transport efficiency, the high conductivity of graphene-based electrodes reduces interfacial losses and shortens charge transport paths. For example, GQD-modified Ag nanowire electrodes increased the short-circuit current density of TENGs by 20-fold [70], while the porous structure and doping-tuned properties of LIGs also enhanced charge storage capacity [70]. Lu et al. [72] further demonstrated that the ionic conductive network within gel-based electrodes accelerates charge migration. This enabled TENG output power reaching 285 volts and 15.5 microamperes, sufficient for sustained charge transfer under low-frequency ocean current fluctuations.

With regard to interface contact optimization, the mechanical flexibility of flexible electrodes contributes to increasing the effective contact area with the triboelectric layer. The wrinkled surface structure of graphene-based electrodes has been demonstrated to enhance the triboelectric effect [70]. The viscoelasticity of gel-based electrodes ensures stable contact under tidal current impacts, while the porous structure of aerogels facilitates charge storage and ion transport [72]. These features have been proven to significantly enhance the surface charge density of TENGs.

Finally, to address the unique demands of ocean energy harvesting, flexible electrodes can achieve synergistic improvements in environmental adaptability and power generation performance through structural modification.

In the context of corrosion-resistant design for marine environments, graphene-based electrodes demonstrate remarkable resilience against corrosion in seawater, attributed to their chemically inert properties. Gel electrodes achieve super hydrophobicity through fluoride modification, thereby preventing contact failure caused by seawater adhesion.

In the context of low-frequency ocean current adaptation, the LIG-based TENG exhibits notable efficacy in capturing mechanical energy from such currents. This capability is attributed to the TENG's porous structure and flexible design, which enable it to achieve a current density of 2.4 μA·cm^{-2} under simulated 0.5 Hz Ocean currents (see Figure 11). The high compressibility of the aerogel electrodes enables the TENG's contact-separation frequency to match ocean current fluctuations, achieving a power density of 4.2 mW·m^{-2}. This result is consistent with the MG-TENG field test data reported by Zhang et al. [73].

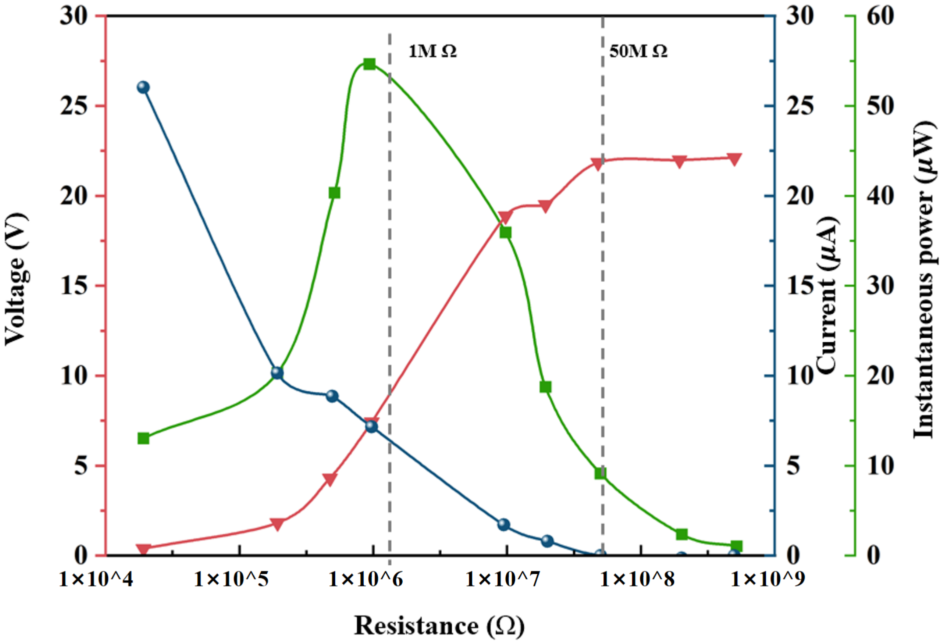

Figure 11. MG-TENG sea trial power density test chart. The data is from [73].

A comparative analysis of key performance metrics reveals that graphene-based electrodes enhance TENG power density by 26% to 513% (As shown in Table 1 of Reference [70]). Through the research of Lu et al. [72], gel-based electrodes have been demonstrated to enhance the stability of the TENG cycle. The performance of these two materials significantly outperforms that of other conventional metal electrodes.

Currently, FOCE-TENG flexible electrodes have been successfully optimized in terms of conductivity, flexibility, and environmental adaptability. However, their practical implementation remains hindered by three fundamental challenges: First, large-scale manufacturing of graphene-based electrodes faces consistency issues. Second, the long-term stability of gel-based electrodes requires improvement, as evidenced by problems such as hydrogel dehydration and insufficient adhesion between organic gels and substrates. Third, the hydrodynamic characteristics of the electrode structure are poorly matched to ocean currents, particularly at low-frequency currents, where contact efficiency and charge output remain sub optimally coordinated. Future research should focus on advancing multi-material composite systems, integrating electrode-friction layer designs, and conducting field validation through offshore experiments to lay the foundation for practical marine applications.

3.2.2. Dielectric Materials

The power generation performance of FOCE-TENG devices is largely determined by the characteristics of the dielectric material employed. As the core functional layer of the device, the surface properties, electrical parameters, and macroscopic and microscopic structural design of this material collectively dictate charge transfer efficiency, charge storage capacity, and long-term power generation stability. To withstand the complex operating conditions of marine environments—including low frequencies, wide flow velocity ranges, and high humidity—optimizing dielectric materials requires a systematic approach that balances multiple critical requirements: flexible adaptability, wear resistance, and energy conversion efficiency. To achieve this goal, a core technical pathway has been established, centered on the sequence of “material selection—structural modification—performance enhancement”. The specific mechanisms of action and related research progress within this pathway can be systematically elaborated.

The fundamental principle guiding dielectric material selection is matching the triboelectric sequence to optimize surface charge transfer. Contemporary mainstream flexible dielectric materials primarily include poly (dichloroethylene methacrylate) (PDMS), polytetrafluoroethylene (PTFE), fluorinated ethylene propylene (FEP), polyvinylidene fluoride (PVDF), and their copolymers. These materials exhibit not only exceptional mechanical flexibility but also outstanding chemical stability, enabling them to withstand periodic bending and vibrational deformation driven by ocean currents. Extensive research indicates that material combinations with greater distance in the triboelectric sequence exhibit more pronounced charge transfer during contact charging. For instance, Cui et al. [74] conducted an experimental study comparing charge transfer between acrylonitrile, Cu, PE, and PTFE, finding that the acrylonitrile-PTFE pairing generated significantly higher charge transfer than other combinations. This finding directly validates the importance of triboelectric sequence matching. To illustrate this, consider the strongly negative material PTFE. When paired with metallic electrodes like aluminum (Al) or copper (Cu), or positively charged materials such as nylon, it exhibits pronounced surface charge separation effects [75]. Similarly, the FEP-PET combination maintains a high and stable potential difference during dynamic contact separation driven by ocean currents [68]. Furthermore, flexible dielectric materials must meet mechanical compatibility requirements in marine environments. Polydimethylsiloxane (PDMS) and polyvinylidene fluoride (PVDF) materials, owing to their low Young’s modulus and high elongation at break, possess the capacity to accommodate deformation demands caused by fluctuations in ocean current velocity [68]. Within this velocity range, the device’s output voltage and current gradually increase with flow speed, effectively preventing power generation degradation due to material fatigue.

Modifying the surface of dielectric materials to optimize contact area is a key method for enhancing charge generation. Topological structures at the micro- and nanoscale, including pores, nanowires, and regular arrays, have been demonstrated to significantly increase surface roughness, thereby amplifying the strength of the triboelectric effect. Researchers Xiao et al. [76] proposed a method utilizing sandpaper as a template to fabricate irregular microporous structures on PDMS surfaces. Their experiments demonstrated that PDMS surfaces patterned with sandpaper of varying grit sizes exhibited irregular pore structures. Pore density increased proportionally with the number of particles, while pore size decreased. Structures formed by specific sandpaper maximized the surface area of the dielectric layer (see Figure 12a), resulting in open-circuit peak voltage and short-circuit current ratios for the corresponding TENG exceeding those of unpatterned samples by more than threefold. Guo et al. [77] fabricated layered nanofiber membranes using electrospinning. The three-dimensional network structure formed by nanoparticles was leveraged to significantly enhance surface roughness. The output voltage of the TENG assembled from this membrane was three times that of a pure polymer membrane (see Figure 12b). It should be noted that in solid-liquid contact-type FOCE-TEGs, excessive roughening of the solid dielectric surface may induce excessive hydrophobicity, thereby reducing output performance for capturing low-frequency ocean current energy [78]. Therefore, surface modification strategies must balance increasing contact area with regulating interfacial wettability.

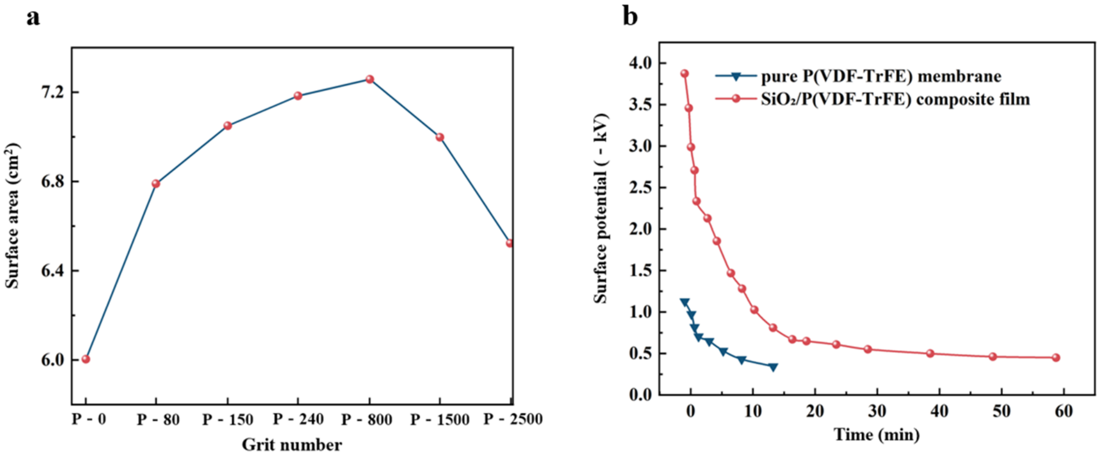

Figure 12. Comparison of Surface Material Effects on Output Performance. (**a**) Surface area of dielectric layer microstructure under different sandpaper grits [76]; (**b**) Surface potential comparison diagram [77].

The optimization of the electrical properties of dielectric materials and the enhancement of their charge storage capacity are imperative for the improvement of output stability. The prevailing contemporary strategy entails the construction of composite dielectric layers through the incorporation of inorganic fillers, with the underlying mechanism elucidated by the surface charge density relationship [77]:

$$\sigma = \frac{\varepsilon_0 \varepsilon_r V_{tri}}{d} \tag{3}$$

Here, σ denotes the surface charge density, ε_r represents the relative permittivity, V_{tri} indicates the triboelectric voltage, and d signifies the thickness of the dielectric layer.

The enhancement of the dielectric constant and the capacity for charge trapping directly boosts surface charge accumulation and storage efficiency. First, the introduction of high-dielectric-constant inorganic fillers, such as $BaTiO_3$, $ZnSnO_3$, and $CaCu_3Ti_4O_{12}$, has been demonstrated to significantly improve the dielectric properties of composite materials. As demonstrated by Kang et al. [79], the dielectric constant of composite films increases with rising filler volume fraction. This results in markedly higher open-circuit voltages for TENG devices compared to pure polymer films. In a similar vein, Wang et al. [80] attained several-fold enhancements in both output current and peak power by strategically incorporating specific nanoparticles into polymers. In addition, innovative fillers that exhibit a combination of high dielectric properties and charge adsorption capabilities have the potential to enhance the peak power density of composite materials by more than tenfold. The superior performance of these fillers is validated by simulation of electric field distribution and output power testing (see Figure 13a) [77]. Secondly, the incorporation of fillers with charge-trapping properties, such as two-dimensional materials including graphene, MoS_2, black phosphorus, and carbon nanotubes, has the potential to mitigate charge dissipation by capitalizing on their abundant charge-trapping sites. As demonstrated by Xiao et al. [76], the optimal doping of the composite dielectric layer with carbon nanotubes led to a substantial enhancement in capacitance, resulting in a notable increase in the peak-to-peak open-circuit voltage and short-circuit current of the respective TENG (see Figure 13b).

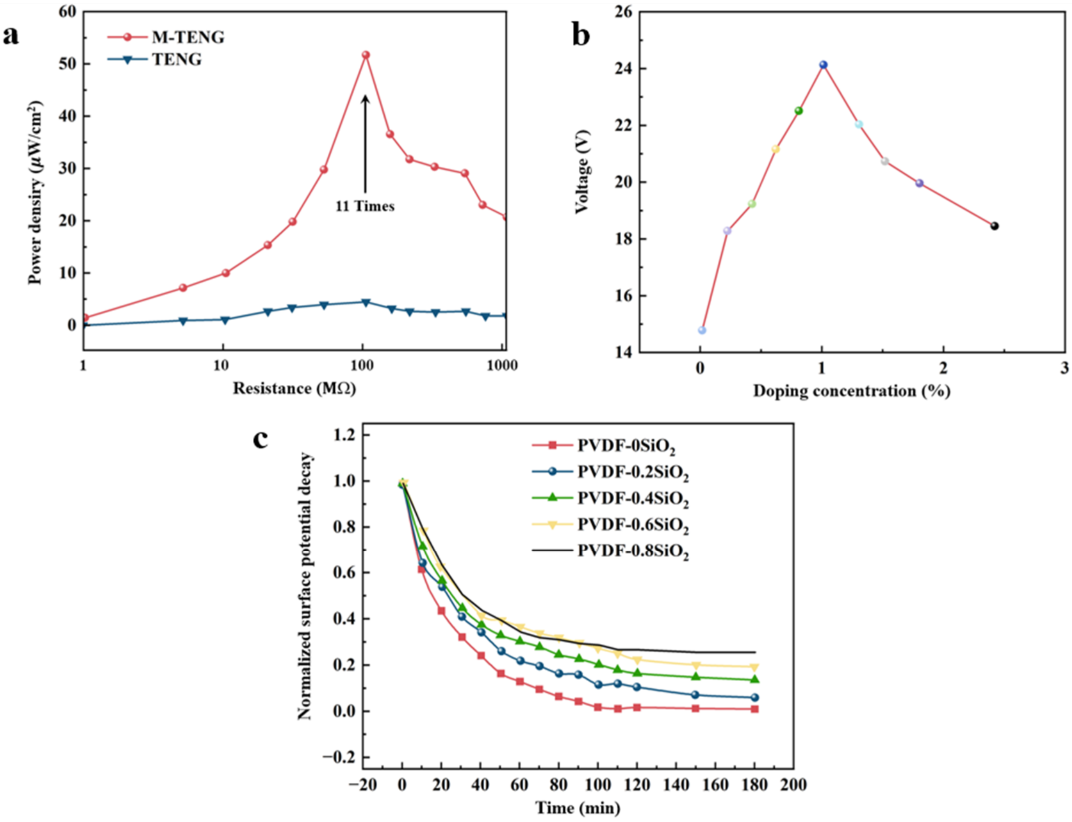

Figure 13. Optimizing the electrical properties of dielectric materials impacts TENG performance. (**a**) Actual power density output of devices based on PDMS and PDMS@F-MOF films [77]; (**b**) Capacitance of micro structured CNT/PDMS dielectric layers with 10 sets of different CNT doping concentrations [76]; (**c**) Surface potential decay curves of PVDF/mSiO_2 nanofibers with varying mSiO_2 concentrations [77].

Kim et al. [81] and Cui et al. [74] have achieved multiple-fold increases in TENG power density by incorporating two-dimensional materials into polymer composites. The incorporation of these fillers led to a simultaneous enhancement in the material's mechanical flexibility, thereby enabling the composite film to withstand tensile and bending deformations and adapt to complex motion patterns driven by ocean currents. Additionally, the incorporation of electret fillers, such as modified SiO_2 nanospheres, facilitates the retention of charge over extended periods and effectively mitigates the decline in surface charge dissipation. As demonstrated by Huang et al. [82], composite nanofiber membranes exhibit a notable retention of their initial surface potential over extended periods (see Figure 13b). In contrast, pure polymer membranes demonstrate a complete dissipation of surface charge. Consequently, the TENG power density based on this composite material is significantly enhanced. Organic-inorganic composite electret materials demonstrate the capacity to accumulate interfacial charges over extensive periods, exhibiting a high degree of charge density retention even under conditions of temperature and humidity fluctuation typical of marine environments. This provides crucial support for the long-term stable operation of FOCE-TENG systems [83–87].

In the structural design of dielectric layers, it is imperative to comprehensively consider the low-frequency and wide-flow-velocity characteristics of ocean current energy, thereby enhancing energy conversion efficiency through structural optimization. The employment of flexible multilayer composite structures has been demonstrated to enhance charge transfer through interlayer synergistic effects. Concurrently, the incorporation of air gaps has been shown to effectively suppress capacitance increase and output voltage attenuation, which are caused by the high dielectric constant of seawater. Zhang et al. [75] conducted an experiment that demonstrated that devices without air gaps exhibited lower output voltages in water. Conversely, the introduction of air gaps significantly boosted output voltage while maintaining stable performance in high-salinity aquatic environments. The phenomenon can be explained by the relevant formula:

$$V_{oc,max} = \frac{\sigma w l}{C_0} \tag{4}$$

Among these, $V_{oc,max}$ denotes the maximum open-circuit voltage of the triboelectric nanogenerator when no external load is applied and the electrodes are separated to the maximum distance from the dielectric layer. It serves as the core metric characterizing the device's output performance. σ represents the surface charge density of the dielectric layer. w and l denote the width and length of the dielectric layer, respectively, whose product constitutes the effective triboelectric contact area $S = w \times l$. C_0 denotes the intrinsic initial capacitance when the device is at its initial position. The core logic of this formula is that the maximum open-circuit voltage is determined by the ratio of the total charge on the dielectric surface ($\sigma \times w \times l$) to the initial capacitance C_0. Therefore, increasing the charge surface density, expanding the effective contact area, or reducing the initial capacitance can all enhance $V_{oc,max}$. This principle also serves as the key theoretical basis for designing the air gap structure of FOCE-TENG in marine environments.

The implementation of an air gap results in a reduction of internal capacitance within the device, thereby leading to a substantial increase in open-circuit voltage for an equivalent charge quantity. Furthermore, the thickness and dimensions of the dielectric layer must align with ocean current dynamics. Thinner dielectric layers have been shown to reduce mechanical losses and enhance response speed. The efficacy of multi-unit FOCE-TENG systems is contingent upon the optimization of effective contact area, which can be achieved by integrating multiple device units in parallel. A direct correlation has been demonstrated between the number of parallel units and the output power of these systems, indicating a linear relationship [68]. For instance, under specific flow rate conditions, the output power of a multi-unit parallel structure has been demonstrated to reach levels sufficient to meet the low-power supply requirements of numerous marine sensors.

In summary, the influence of dielectric materials on FOCE-TENG power generation performance follows a three-dimensional synergistic regulation pattern: material properties, structural design, and environmental adaptation. Surface microstructure modification primarily enhances charge generation by increasing contact area, while the incorporation of high-dielectric-constant fillers and charge-trapping fillers optimizes electrical properties to enhance charge storage. Electret modification and composite structural design are focused on ensuring long-term operational stability under harsh ocean current conditions. The extant research conclusively demonstrates that composite dielectric materials achieve significantly superior performance optimization compared to single-material systems. The combination of two-dimensional materials with high-dielectric fillers in synergistic doping strategies has been demonstrated to enhance device power density by up to tens of times. Following extended periods of operation, FOCE-TENG exhibits consistent electrical parameter stability, thereby substantiating its notable durability. Future research should concentrate on the development of seawater-resistant, durable, and flexible composite dielectric materials while achieving a better balance between mechanical flexibility and energy conversion efficiency. This will effectively advance the practical application of such generators in marine distributed energy systems [88–92].

3.2.3. Surface Micro-Nano Structure

The core of FOCE-TENG performance optimization lies in regulating the surface micro-nano structures of its friction layer, which is a key approach to enhancing energy conversion efficiency. By precisely controlling surface topography, the contact state, charge transfer, and mechanical compatibility at solid-solid/liquid interfaces can be effectively optimized, thereby overcoming performance limitations in low-frequency ocean current environments. Research indicates that micro/nano-structured surfaces significantly enhance device output performance through mechanisms such as increasing effective contact area, regulating interfacial wettability, and amplifying triboelectric effects. Furthermore, this approach endows devices with outstanding structural compatibility, potential for large-scale fabrication, and adaptability to marine environments [93–97].

The preparation of surface micro- and nano-structures requires balancing the mechanical properties of flexible substrates, corrosion resistance in marine environments, and scalability for mass production. Currently, two primary technical approaches are employed: First, methods characterized by simple processes and stable mechanical properties, such as the technique by Zhao et al. [98] that utilizes sandpaper of varying grit sizes to polish linear microgrooves onto surfaces like aluminum foil and polyimide. This method offers advantages including low cost, suitability for large-area fabrication, and potential for industrial implementation. The second approach employs photolithography replication techniques. Zhao et al. [99] fabricated silicon templates via photolithography and transferred them onto polymers like PDMS, achieving high-precision surface topography suitable for optimizing solid-liquid interfaces.

In practical marine applications, the modified devices demonstrate significant performance enhancements: for instance, the large-scale device in Zhao et al.'s [98] experiment achieved an output of 1500 V and 75 μA, with a power density of 62.3 $\mu W/cm^2$; the solid-liquid interface device in Zhao et al.'s [99] work saw its output voltage increased to 27.2 V, capable of driving hundreds of LEDs. Simultaneously, the devices demonstrate excellent environmental adaptability. For instance, Chen et al. [100] observed less than 8% performance degradation after 30 days of immersion for PTFE composite structures, while linear structures reduced biofouling rates by 40%.

Despite ongoing technological advancements, micro- and nano-structures still face several critical challenges, primarily including [101]: insufficient mechanical stability under long-term erosion (typically with a service life of less than one year), sensitivity of solid-liquid interface wettability to variations in seawater salinity and temperature, and difficulty in controlling surface structural uniformity across large-area devices [102–106]. Future research should focus on developing mechanically adaptive biomimetic structures, constructing multiscale composite morphologies suited for wide-range ocean current environments, and advancing scalable continuous manufacturing technologies to accelerate the engineering application of FOCE-TENG.

3.3. The Impact of Network Configuration on Power Generation Performance

Although a single FOCE-TENG unit has achieved power generation capability through component optimization, its limited output power struggles to meet the energy demands of practical applications such as the ocean Internet of Things [107–111]. Therefore, integrating multiple units into arrays or networks (Figure 14) is a key strategy for realizing efficient, large-scale "blue energy" capture. It is important to note that the overall performance of an array is not a simple summation of individual unit outputs [112–116]. Instead, it is synergistically influenced by network topology, phase relationships between units, and energy management strategies [117–121]. Consequently, in-depth research into network configurations is crucial for advancing the practical application of FOCE-TENG systems.

The fundamental electrical connection topologies primarily include series and parallel configurations [122–126]. Series connections enhance the total open-circuit voltage, theoretically summing the voltages of each cell, but the total output current is limited by the cell with the lowest current in the network. Parallel connections aim to increase the total output current, theoretically summing the total charge transfer across all cells, while the output voltage is clamped to the level of a single cell [127]. He et al. systematically investigated the output characteristics of series/parallel TENGs, confirming the gain effects of different configurations on voltage and current [128]. The choice of connection method depends on the specific voltage or current requirements of the application.

In actual marine environments, the spatiotemporal inhomogeneity of ocean currents makes it difficult for individual units within a FOCE-TENG array to maintain synchronized motion, resulting in phase differences among alternating current signals [4]. If such out-of-phase units are directly connected in parallel, their positive and negative voltages will cancel each other out. This not only hinders effective energy superposition but also causes significant internal energy dissipation, substantially reducing the overall output efficiency of the network [127]. To address this issue, the mainstream approach involves rectifying the AC output of each TENG unit before parallel connection, converting it to DC to avoid phase cancellation and achieve stable energy accumulation [129–133]. Additionally, Liu et al. [127] proposed a large-scale wave energy harvesting grid structure based on optimized TENG network topology, providing theoretical guidance for enhancing energy capture efficiency under complex ocean conditions.

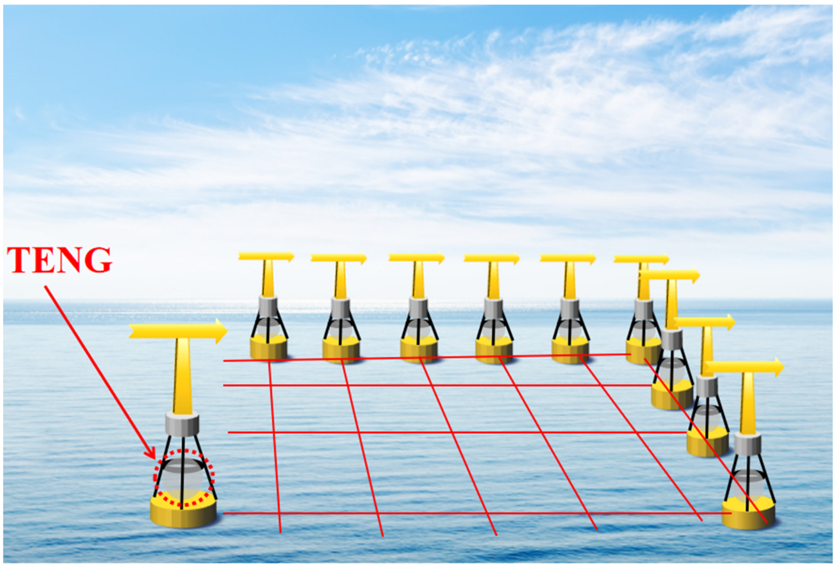

Figure 14. Multiple FOCE-TENG units integrated into arrays or networks.

In addition to optimizing fundamental electrical connection methods, more advanced network configurations and management strategies have been extensively explored. On one hand, configuration innovations represented by modular designs enable flexible integration of multiple TENG units, facilitating large-scale deployment and maintenance, such as the O-ring modular TENG system [134]. On the other hand, the synergistic integration of efficient power management circuits with TENG networks is indispensable [129,135]. These circuits are specifically designed for the pulsed high-voltage, low-current output characteristics of TENGs, enabling efficient energy harvesting, storage, and regulation. Their performance has been validated in multiple studies [136–140]. Developing universal passive power management strategies to ultimately construct “self-powered” TENG networks capable of supplying power to their own management circuits and loads is a current research focus in this field [135,136].

In summary, the networking of FOCE-TENG devices is a critical step in the process of expanding from individual components to large-scale energy harvesting systems. Research in this field is continually progressing, from fundamental series-parallel connections to addressing asynchronous excitation issues in real ocean environments, and further to network topology optimization and modular design [127,134]. In the future, the design of FOCE-TENG network architectures must evolve in tandem with efficient power management strategies. It is imperative to recognize that the comprehensive optimization of this system is paramount to fully actualize its considerable potential as a distributed marine energy solution. This will ensure the provision of sustainable power support for ocean exploration and monitoring equipment [141–145].

4. Collaborative Testing System and Performance Validation

The FOCE-TENG performance control framework established in the preceding section encompasses theoretical modeling, core component optimization, and network design. Its effectiveness requires validation through systematic testing. Given the dynamic characteristics of ocean current environments, the complexity of flow-induced vibrations, and the tight coupling among various performance parameters, it is imperative to construct an experimental system capable of simultaneously monitoring flow field parameters, vibration responses, and electrical outputs. This chapter details the core components and design strategy of this test system. Collaborative testing quantifies the performance regulation effects, providing empirical evidence for technological optimization while demonstrating the adaptability and stability of FOCE-TENG in real ocean environments.

4.1. Testing Core Components of the System

The overarching objective of the collaborative testing system is to achieve precise synchronous measurement of three types of parameters: flow field, vibration, and electrical properties. The system’s overall performance is contingent upon the selection and mutual compatibility of key modules [146–150]. The system is composed of three modules: a flow field simulation module, a vibration monitoring module, and an electrical testing module. It is imperative that each module meet both high-precision and high-synchronization requirements. This is necessary to ensure the reliability and repeatability of test results.

The flow field simulation module is principally employed to reproduce steady-state or dynamic water currents under low-velocity conditions in marine environments. The core components of the system consist of a recirculating water tank, water pumps, and a flow velocity calibration unit. The configuration and performance parameters of this module have been validated through numerous experimental apparatus studies and publicly available scientific facility information [151–155]. The recirculating water tank is a fundamental flow field simulation platform that provides a continuous and stable flow environment. This capability has been explicitly applied in marine engineering-related experiments, supporting long-term, multi-objective measurements of hydrodynamics and detailed flow fields [156–160].

As demonstrated in Figure 15, Ni et al. [161] employed a standard flume as the experimental apparatus, measuring 16 m in length, 0.4 m in width, and 0.4 m in height, with a flow velocity adjustment range of 0.2–0.7 m/s. The findings indicated that this velocity range is consistent with the low-velocity simulation capabilities of existing multifunctional wave-wind-current integrated flumes, thereby demonstrating its potential to meet the testing requirements for vortex-induced vibration of marine structures within this velocity interval. Furthermore, the repeatability error of this recirculating flume is less than 1.0%, indicating a high degree of stability. The velocity deviation control standards for analogous research facilities further substantiate its aptitude for long-term stability testing.

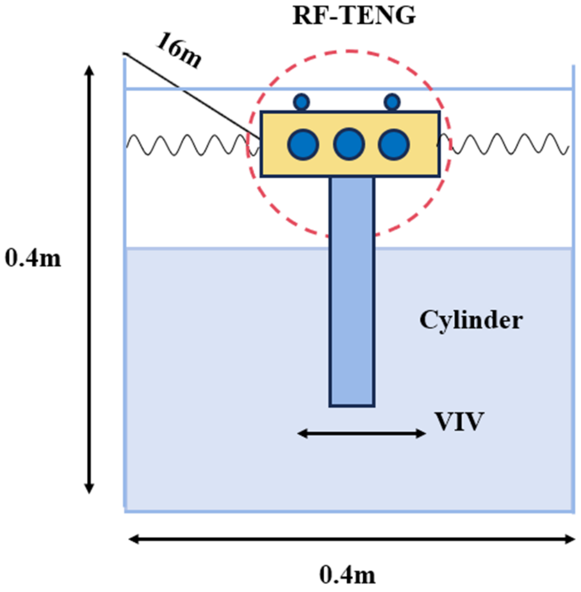

Figure 15. Schematic diagram of the experimental setup by Ni et al. [161].

In experimental scenarios necessitating precise measurement and control of lower flow velocities, Zhang et al. [162] employed an SCP-180 programmable water pump to simulate real-world flow conditions. Concurrently, the flow velocity within the pipeline was meticulously monitored and real-time feedback was systematically provided using an advanced LS300-A high-precision flowmeter. The research team then systematically completed comprehensive electrical output performance testing of the triboelectric soft fish tail device across a flow velocity range of 0.24 m/s to 0.89 m/s, building upon this precisely controlled flow field.

The data from Zhang et al. [162] show that as the flow velocity gradually increases from 0.24 m/s to 0.89 m/s, the open-circuit voltage steadily rises from 200 V to 313 V. Correspondingly, the short-circuit current increases from 1.65 μA to 3.18 μA. Specifically, at a flow velocity of 0.89 m/s, researchers calculated the device's volumetric power density to be 5.56 W/m³ using the power formula $P = I^2R$ (where P is instantaneous power, I is current, and R is the matched load resistance;). The experimental system's efficacy is evidenced by its ability to attain stable regulation within the target flow velocity range and precise calibration of flow field parameters.

Furthermore, at a constant flow velocity of 0.89 m/s, the charge transferred per cycle by the triboelectric soft fishtail device exhibited stability at 0.17 μC. The repeatability and stability of this electrical parameter further corroborate the high reliability of the flow velocity measurement scheme and system calibration results.

Moreover, in select studies that emphasize the mechanisms of cross-medium energy conversion, open-loop wind tunnels are frequently utilized to simulate stable airflow environments. For instance, Kim et al. [163] explicitly defined the wind tunnel test section geometry as 0.6 m wide, 0.6 m high, and 1.4 m long, with wind speed adjustable from 2.9 to 9.1 m per second. This standardized configuration provides an effective experimental platform for systematically investigating flow-induced vibration phenomena and conducting comparative analyses.

The research team employed this wind tunnel system to conduct a systematic investigation into the unique rapid flipping flow-induced vibration behavior exhibited by buckling elastic thin plates under aerodynamic loading. The fundamental experimental configuration and testing methodology are illustrated in Figure 16. This schematic illustrates the dynamic process of the elastic plate switching between two stable configurations under aerodynamic loading, thereby validating the wind tunnel platform's precise simulation capability for such complex fluid-structure interaction phenomena. The validity of the wind speed range is further substantiated by experimental data from Figure 16b,c. The horizontal axes of both figures explicitly indicate that the primary wind speed range examined in the experiment's spans from 6.2 to 9.1 m per second. The figures also include reliable test data from the low-wind-speed segment, comprehensively covering the core range of 2.9 to 9.1 m per second. This finding substantiates the practical utility of this wind tunnel configuration in real-world research applications.

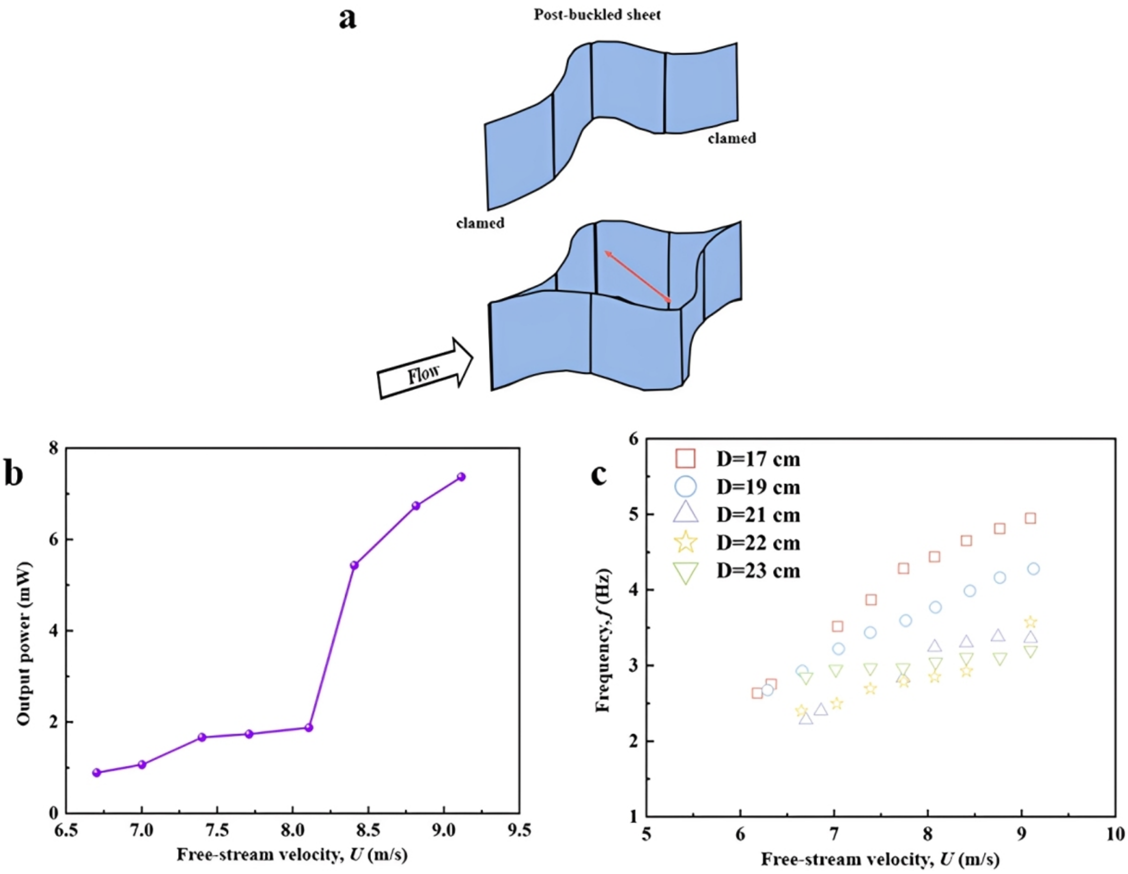

Figure 16. (**a**) Schematic diagram of flow-induced periodic snap-through; (**b**) Relationship between external load output power and wind speed; (**c**) Oscillation frequency versus free-stream velocity at five wall distances. Data sourced from [163].

From an intrinsic mechanism perspective, the wind tunnel simulation experiments in this study are grounded in the principles of fluid-structure interaction dynamics. By employing modified static equilibrium equations to describe the buckling behavior of thin plates, this work theoretically elucidates the multi-force equilibrium relationship among aerodynamic forces, internal bending restoring forces, axial forces, boundary constraint forces, and contact forces. Notably, this fundamental principle shares essential commonalities with the interaction laws between fluids and flexible structures in aquatic environments: both involve periodic or non-periodic structural vibrations induced by fluid driving forces, and their dynamic equilibrium mechanisms can be described through models coupling structural mechanics and fluid mechanics. Therefore, the open-loop wind tunnel test configuration, key parameter settings, and fluid-structure interaction simulation framework adopted in this study provide direct reference and basis for the design and optimization of water flow environment testing systems for marine energy harvesting [163–167].

4.2. Collaborative Test Design Strategy

In order to accomplish the primary objective of unveiling the multiphysics coupling mechanisms among flow field, vibration, and electrical properties through collaborative testing, it is essential to methodically arrange and construct the formulation and implementation of the overall design strategy around three fundamental aspects: parameter control, synchronous data acquisition, and environmental adaptation.

At the level of parameter control, the testing system must possess the capability to implement high-precision regulation of multiple categories of parameters to support multidimensional collaborative performance evaluation and analysis. Specifically, flow field parameter control is achieved by adjusting water flow velocity or wind speed. This adjustment enables the simulation of ocean wave energy environments with varying energy intensities. The flow velocity control range for the TE-SFT device testing spans from 0.24 to 0.89 m per second (m/s), while for the VMG-TENG device testing, the range is from 0.3 to 0.6 m/s. A minimum trigger velocity of 0.2 m/s is required. The corresponding output performance has been experimentally validated in Figure 17a–d [42,162]. Conversely, wind speed regulation primarily targets the range of 2.9–7.8 m/s, encompassing various wind conditions from light breezes to strong winds. The voltage, current, and charge output characteristics of the FIV-TENG device within this wind speed range are intuitively illustrated in Figure 17e–g. The theoretical foundation of this model is predominantly derived from the rotational kinetic energy formula (Equation (5)) and the oscillator motion equation (Equation (4)).

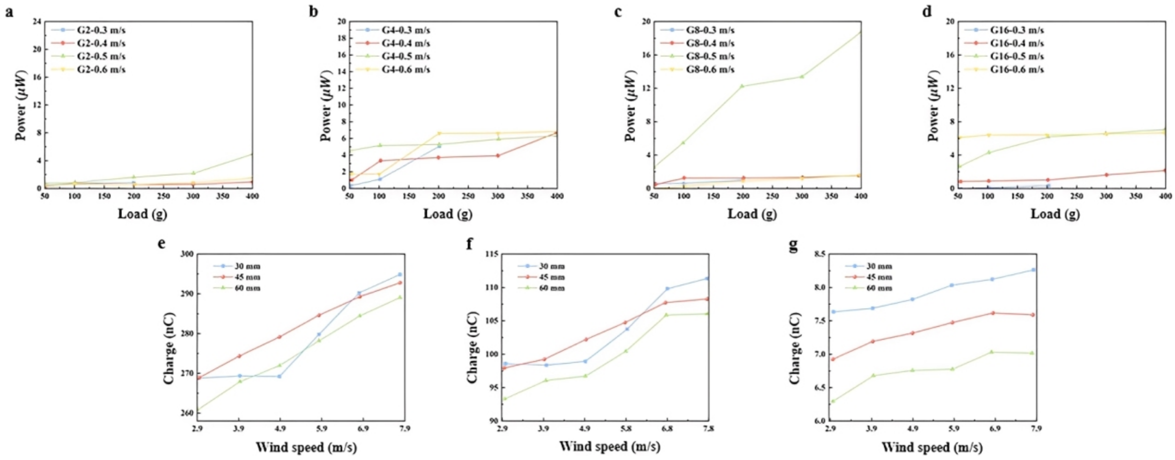

Figure 17. (**a**–**d**) Power-load relationship of VMG-TENG at different flow velocities [42]. (**e**–**g**) Output comparison at different cantilever lengths [64].

With respect to structural parameter regulation, research is chiefly concentrated on modifying the physical configuration of energy harvesting devices themselves to explore the intrinsic relationship between structural optimization and system synergistic performance. Specifically, Li et al. [42] modulated flow field interactions by systematically varying the number of gratings (2–16); Zeng et al. [64] concentrated on optimizing cantilever beam length parameters (30–60 mm); Zhang et al. [162] innovatively designed the inclination angle of an inertial pendulum (0–8°); while Ni et al. [162] altered the internal structure by controlling the packing density of particulate matter (26.3–100%). The performance impacts of these parameter adjustments have been thoroughly validated through corresponding experimental data. As demonstrated in Figure 17, the impact of grid count on MG-TENG output performance is evident. The 8-grid structure is observed to exhibit optimal overall performance. The optimization results for cantilever length are substantiated in Figure 17e–g, where a 45 mm length simultaneously achieves linear output response and high stability.

Signal synchronous acquisition serves as the critical technological foundation for collaborative testing, with its core objective being the strict temporal synchronization of flow fields, vibrations, and electrical signals. Existing systems typically employ a combination of hardware triggering and software coordination to ensure precise temporal alignment. On the hardware side, a single trigger source synchronously controls flow field drivers, displacement sensors, and electrical measurement equipment, adjusting inter-channel trigger delays to within 1 millisecond. Software-wise, unified acquisition programs developed on integrated platforms like LabVIEW or MATLAB enable simultaneous collection, timestamp alignment, and storage of vibration displacement, contact force, and electrical signals. The sampling frequency is uniformly set to 2000 Hz, providing a reliable data foundation for subsequent multi-parameter correlation and mechanism analysis [162].

Taking the FIV-TENG test as an example, the synchronous acquisition of wind speed, vibration frequency, and open-circuit voltage, combined with the correlation formula between system vibration and fluid forces (Equation (4)), reveals the regulatory mechanism of flow field parameters on vibration behavior. Furthermore, experiments by Zeng et al. [64] demonstrated that increasing wind speed from 2.9 m/s to 7.8 m/s correspondingly raised the vibration frequency, boosting output power from 0.9 mW to 1.3 mW (as shown in Figure 18). This result directly validates the prevailing hypothesis of strong coupling between flow field, vibration, and electrical performance.

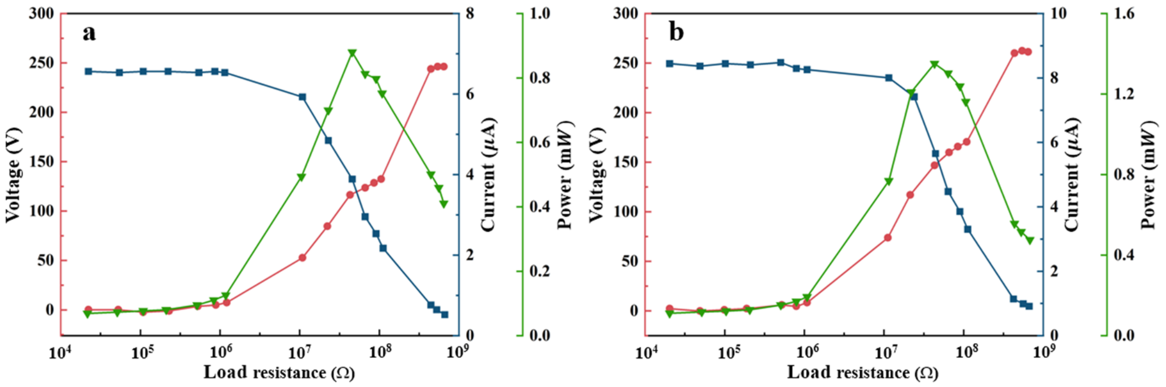

Figure 18. Output performance of the FIV-TENG. (**a**) Voltage, current, and corresponding output power of the FIV-TENG under different external load resistances at a wind speed of 2.9 m/s; (**b**) Voltage, current, and corresponding output power of the FIV-TENG under different external load resistances at a wind speed of 7.8 m/s. The data comes from [64].

In experimental studies of VC-TENG, Yu et al. [168] established a theoretical model based on classical vortex-induced vibration dynamics equations and obtained crucial experimental evidence by simultaneously monitoring vortex shedding intensity, structural amplitude, and charge transfer rate. The study demonstrated that after adopting an optimized curved wind plate design, the charge transferred per cycle increased significantly from 0.01 μC to 0.47 μC—a 47-fold increase—while the structural vibration amplitude also markedly intensified. This comparative experimental result clearly reveals the intrinsic mechanism whereby flow field structural regulation can effectively enhance vibration behavior, thereby synergistically improving power generation performance.

Given the extreme complexity and harshness of the actual marine environment, the design and validation of the testing system must prioritize environmental adaptability as a core evaluation criterion. The verification framework under consideration is comprised of two primary dimensions: waterproof sealing performance and long-term operational stability.

In order to assess the waterproof performance of a product, researchers generally establish controlled simulated rainfall test platforms or conduct long-term continuous immersion tests. By means of these tests, they are able to systematically evaluate the protective efficacy of device packaging and sealing structures in humid environments. Specifically, Zeng et al. [64] conducted simulated rainfall tests on FIV-TENG devices featuring a trapezoidal cylindrical shell sealing structure. The edges were reinforced with waterproof tape to effectively prevent liquid water from penetrating the structure. The device's open-circuit voltage output demonstrated no substantial deviation when subjected to heavy rainfall conditions, with a maximum recorded intensity of 33.9 mm per hour. This performance retention rate of 96.8% is noteworthy, particularly when considering the potential impact of severe weather conditions on the device's functionality. Concurrently, Zhang et al. [162] exposed TE-SFT devices to a 30-day continuous immersion test. The integrated sealing structure, fabricated using advanced soft material synthesis technology, demonstrated outstanding resistance to long-term water environment erosion. As shown in Figure 19, following a 30-day period of immersion, the device exhibited an open-circuit voltage retention rate of 96.81%, thereby substantiating the reliability of its sealing design.

With regard to the evaluation of long-term operational stability, the study undertook a comprehensive assessment of durability. This was achieved by meticulously monitoring the attenuation trends of vibration response and electrical output performance over extended periods or cycles. These observations were made while the device was operated under strictly controlled conditions. For instance, Yu et al. [168] conducted a continuous operation test of VC-TENG devices for 6.9 h at a wind speed of 4.1 m/s. After undergoing 11,200 operational cycles, the retained charge transfer efficiency remained at 97.9%, with overall electrical performance degradation below 5%. Zhang L et al. [43] conducted a 7000-s continuous operation of VIV-TENG devices at a wind speed of 3.68 m/s, accumulating approximately 98,000 cycles. As demonstrated in Figure 20, the device's open-circuit voltage waveform exhibited remarkable stability throughout the testing period, with no substantial degradation observed. This exceptional stability is attributable to the establishment of a stable coupling mechanism between internal vibrations and electrical output within the device. Zhang et al. [43] elucidated the synergistic relationship among hydrodynamic forces, structural vibration, and charge transfer through the use of coupled dynamic equations. Yu et al. [168] optimized structural parameters based on models of vortex-induced vibrations. This ensured stable vibration excitation intensity and energy conversion efficiency during long-term operation. This provides fundamental assurance for reliable application in real marine environments.

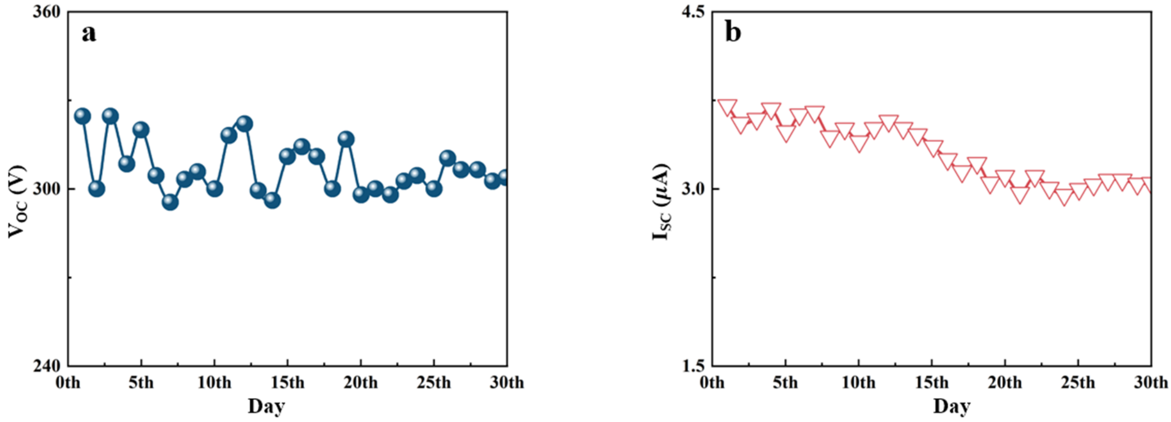

Figure 19. Water immersion durability of TE-SFT at v = 0.89 m/s. (**a**) Voltage; (**b**) Current. Data from [162].

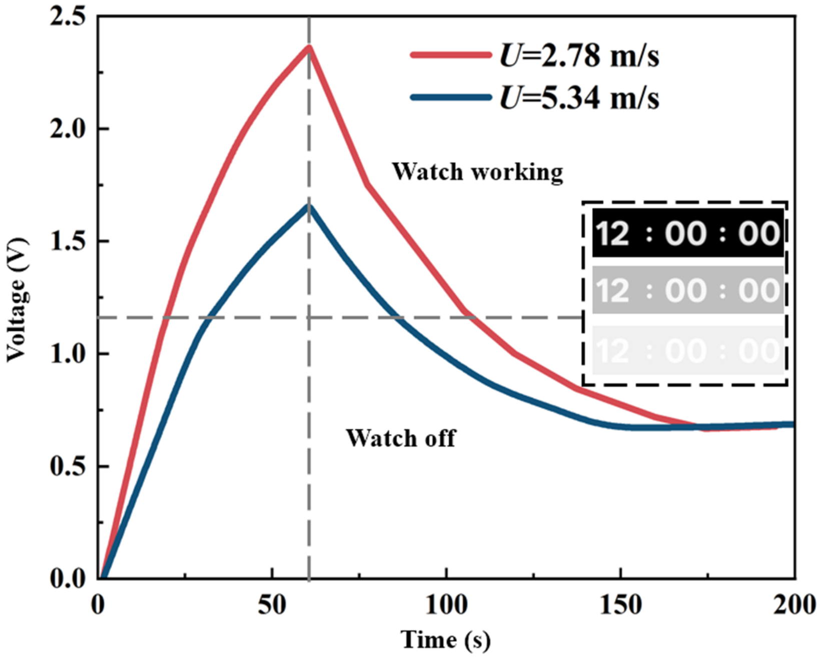

Figure 20. Charging performance and application demonstration of T-VIV-TENG for powering digital watches. Data sourced from [43].

Furthermore, certain test systems incorporate ambient temperature and humidity as pivotal variables to validate the performance robustness of devices under more extensive environmental conditions [169–173]. Test results by Zhang et al. [162] for TE-SFT devices (as shown in Figure 21) indicate that no significant fluctuations were observed in open-circuit voltage, short-circuit current, or charge transfer within the temperature range of 10–35°C and relative humidity range of 35–85% RH. This finding suggests that the material system and structural design of the device can effectively withstand the dynamic temperature and humidity variations commonly encountered in marine environments [174–178], further expanding its potential application scenarios.

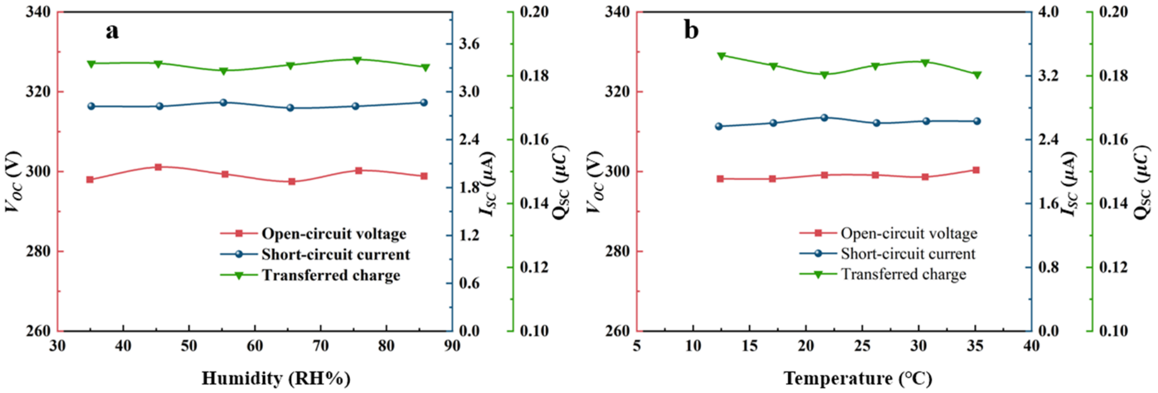

Figure 21. Under conditions of $f = 0.85$ Hz, $\alpha = 45°$, and o = 8°. (**a**) Electrical output performance of the TE-SFT at different humidity levels; (**b**) Electrical output performance of the TE-SFT at different temperatures. Data sourced from [162].

Existing studies have reported performance data for FOCE-TENG devices across various structural and material configurations. However, direct comparisons are significantly limited due to factors such as the test fluid medium (seawater/air), flow velocity range, and device dimensions. Table 4 summarizes the normalized performance metrics of mainstream FOCE-TENG devices, uniformly normalized based on device area/volume, with key test conditions noted. Results indicate that triangular-section oscillators and biomimetic flexible structures exhibit superior power density at low flow velocities, providing quantitative references for subsequent device structural optimization. Future research should establish unified performance evaluation standards and testing protocols to advance this technology from laboratory development to engineering applications.

Table 4. Standardized performance comparison table for FOCE-TENG and similar ocean current energy conversion technologies.

Configuration	**Flag-Type [45]**	**Thin-Film Type [68]**	**Bionic Fish Tail [162]**	**Fully Encapsulated [64]**	**Trapezoidal Vibrator [66]**
Structure	Blunt Body—Flexible Flag	Multilayer Thin Film Array	Sealed Oscillating Structure	Trapezoidal Oscillator—Cantilever	Triangular-section blunt body
Operating conditions	Low seawater flow velocity	Flow Field—Frequency Modulation	Long-term soaking	Airflow Simulation	Equivalent flow velocity
Normalization Basis	Power Density (Area)	Charge/Efficiency (per unit area)	Volume power density	Power density (windward area)	Amplitude/Efficiency (Characteristic Dimensions)

5. Limitations and Prospects

The theoretical foundation, control technology, and testing methods of FOCE-TENG have formed a comprehensive technical system, with its feasibility in capturing low-velocity ocean currents experimentally validated. However, transitioning from laboratory research to large-scale engineering applications still faces practical challenges such as extreme environmental adaptability, technical bottlenecks in scaling up, and balancing material costs.

5.1. Technical Limitations

5.1.1. Insufficient Adaptability to Extreme Marine Environments

The impact of deep-sea high-pressure environments on the charge transfer mechanism of FOCE-TENG remains unclear. It is hypothesized that high pressure may degrade the dielectric properties of the friction layer and exacerbate charge dissipation, thus limiting its application potential in deep-sea environments. Marine biofouling has been shown to compromise the integrity of friction surfaces and disrupt mechanical motion, while existing antifouling coatings have been found to struggle to maintain long-term protective efficacy. Furthermore, ocean currents demonstrate wide velocity fluctuations (0.5–3.6 m/s) and complex flow directions, resulting in a significant reduction in energy capture efficiency in non-resonant states. Existing devices encounter difficulties in achieving stable output across the entire velocity range.

5.1.2. Scalable Deployment Faces Technical Bottlenecks

Large-scale FOCE-TENG arrays encounter challenges in terms of synchronization control. Spatial inhomogeneity in ocean currents gives rise to varying vibration phases across individual units, rendering direct parallel connection susceptible to mutual energy cancellation. Existing energy management systems demonstrate an inadequate alignment with the high-voltage, pulsed, low-current output characteristics of TENGs, resulting in suboptimal energy conversion and storage efficiency. Moreover, the deployment of arrays is associated with considerable installation expenses and challenges related to maintenance. The absence of modular integrated designs that are well-suited to marine environments contributes to the limited adoption of this technology on a large scale.

5.1.3. The Trade-Off between Material Properties and Cost

The elevated expense of large-scale manufacturing for contemporary high-performance materials (e.g., graphene composites and fluoropolymers) continues to be a significant barrier, constraining their engineering applications. The optimization of both long-term corrosion resistance and mechanical stability is a challenging undertaking, particularly when considering their synergistic relationship. Metal electrodes are susceptible to corrosion caused by seawater, while flexible polymers tend to fatigue and fail under sustained dynamic loads. Additionally, poor interface compatibility between high-dielectric-constant fillers and flexible substrates prevents simultaneous enhancement of charge storage capacity and mechanical flexibility in composite dielectric materials.

5.1.4. Failure Modes and Reliability Shortcomings in Extreme Marine Environments

In deep-sea high-pressure environments, dielectric materials experience reduced charge trapping capacity due to pore compression, leading to charge dissipation and output attenuation. Simultaneously, high pressure exacerbates fatigue in flexible structures, causing unstable friction contact. Marine biofouling covers the friction layer surface, reducing its roughness and hindering charge transfer. Concurrently, microbial metabolites synergistically accelerate electrode corrosion, collectively resulting in sustained output performance degradation. Moreover, wide-amplitude ocean current fluctuations readily displace energy harvesters from their resonant operating range. Traditional passive tuning structures struggle to adapt to sudden velocity changes, often causing “resonance loss” and power supply interruptions. The coupled effects of high pressure, biofouling corrosion, and dynamic flow fields severely limit the long-term reliability and environmental adaptability of marine energy harvesting devices.

The transition of FOCE-TENG from laboratory research to large-scale engineering applications is constrained by three core technical bottlenecks: insufficient extreme environmental adaptability, scalable deployment challenges, and the trade-off between material properties and cost. To address these bottlenecks in a targeted and actionable manner, next section reorganizes future research directions into short-term, medium-term, and long-term priorities, establishing clear connections between each priority and specific technical pain points.

5.2. Future Priorities

To advance flow-induced vibration triboelectric nanogenerators from proof-of-concept to practical application, a systematic phased research plan must be established. The following outlines the core objectives, implementation pathways, and anticipated contributions for short-term, medium-term, and long-term phases. Each phase builds upon the preceding one, forming a progressive R&D trajectory.

5.2.1. Short-Term Priorities

This phase aims to address the core bottlenecks constraining the field validation and initial application of the technology, focusing on enhancing device performance in real ocean environments, establishing a comparable evaluation system, and improving short-term environmental reliability. First, to address the low energy capture efficiency and unstable output across wide flow velocity ranges in existing devices, it is imperative to refine multiphysics-coupled flow-induced vibration theoretical models. Based on this, optimize key structural parameters and introduce passive flow velocity adaptation mechanisms to significantly broaden the efficient operating range. This will ultimately lead to the development of practical devices capable of stable power output at low flow velocities. Second, to overcome the challenges of inconsistent testing platforms and evaluation standards that hinder research comparability and slow technological iteration, efforts should focus on establishing standardized testing environments and procedures. This includes defining key performance indicators and developing integrated universal testing platforms to create universally recognized performance testing and evaluation norms, thereby providing benchmarks for technological advancement. Finally, to address the challenge of short-term performance degradation caused by marine biofouling and corrosion, advanced anti-fouling coating technologies should be applied, sealing and encapsulation processes optimized, and accelerated aging tests conducted for validation. These measures will substantially enhance the short-term durability and reliability of devices in marine environments.

5.2.2. Mid-Term Research Priorities

Mid-term research will shift its focus to laying the groundwork for large-scale application, centered on overcoming cost constraints of high-performance materials, developing efficient modular integration strategies, and introducing intelligent design tools. Currently, the conflict between material cost and performance is prominent. Therefore, it is necessary to explore new low-cost, high-durability composite dielectric materials and flexible electrode systems, while developing corresponding large-scale fabrication processes to achieve practical materials with an optimal balance between cost and comprehensive performance. Simultaneously, to bridge the gap from single devices to array systems, solutions must address energy cancellation within array cells caused by uneven flow field distribution and the mismatch between pulsed outputs and energy management circuits. This requires designing standardized modular units, adopting advanced array topologies and power management architectures, and developing modular array systems with significantly enhanced output power that are easy to deploy and maintain. Furthermore, to overcome the limitations of inefficient traditional empirical design approaches, a multi-parameter design database should be established. Machine learning methods should be employed to train performance prediction models, enabling the development of intelligent design-aids. This will facilitate rapid structural optimization and performance forecasting for devices, substantially shortening the R&D cycle.

5.2.3. Long-Term Research Focus

The long-term goal is to advance this technology toward deep-sea and large-scale engineering applications while expanding its functional boundaries. The primary challenge lies in adapting devices to extreme high-pressure environments in the deep sea. This requires in-depth exploration of charge dynamics under multi-field coupling effects such as high pressure and low temperature. Based on these findings, high-pressure-resistant devices with specialized structures and packaging designs must be developed to ultimately enable reliable application in fields like deep-sea observation. Second, to address engineering bottlenecks in large-scale array deployment—such as high costs, maintenance difficulties, and complex energy management—floating modular array systems must be developed. These systems should integrate IoT and edge computing technologies for intelligent monitoring and dynamic energy allocation, while exploring self-powered energy management solutions. This approach will establish large-scale ocean energy harvesting networks that deliver sufficient power output for practical needs while ensuring economic viability and maintainability. Finally, to enhance the technology's comprehensive value, it should transcend single-function energy harvesting by exploring integration with sensing technologies to develop self-powered multi-parameter ocean environment sensors. Concurrently, research should focus on complementary advantages with other energy harvesting mechanisms like piezoelectric and electromagnetic technologies to construct broadband, high-efficiency hybrid energy harvesting systems. This will enable multifunctional integrated applications within the marine Internet of Things.

Author Contributions

K.Y. (Kefan Yang): conceptualization, methodology, software; Y.Z. (Yi Zhang): data curation, writing—original draft preparation; S.Z.: visualization, investigation; K.Y. (Keqi Yang): formal analysis; Y.M.: software, validation; Y.Z. (Yixuan Zeng): paper revision; D.Z.: supervision, writing—reviewing and editing. All authors have read and agreed to the published version of the manuscript.

Funding

This study is supported by the Fund of Guangdong Provincial Key Laboratory of Intelligent Equipment for South China Sea Marine Ranching (Grant No. 2023B1212030003).

Institutional Review Board Statement

Not applicable.

Informed Consent Statement

Not applicable.

Data Availability Statement

Not applicable.

Conflicts of Interest

The authors declare no conflict of interest.

Use of AI and AI-Assisted Technologies

No AI tools were utilized for this paper.

References

1. Davis, A.; Chang, H. Underwater Wireless Sensor Networks. In Proceedings of the 2012 Oceans, Hampton Roads, VA, USA, 14–19 October 2012. https://doi.org/10.1109/OCEANS.2012.6405141.
2. Luo, J.; Chen, Y.; Wu, M.; et al. A Survey of Routing Protocols for Underwater Wireless Sensor Networks. *IEEE Commun. Surv. Tutor.* **2021**, *23*, 137–160. https://doi.org/10.1109/COMST.2020.3048190.
3. Al Guqhaiman, A.; Otoom, M.; Aljaedi, A.; et al. A Survey on MAC Protocol Approaches for Underwater Wireless Sensor Networks. *IEEE Sens. J.* **2020**, *21*, 3916–3932. https://doi.org/10.1109/JSEN.2020.3024995.
4. Huang, X.; Sun, S.; Yang, Q. Data Uploading Strategy for Underwater Wireless Sensor Networks. *Sensors* **2019**, *19*, 5265. https://doi.org/10.3390/s19235265.
5. Yao, L.; Du, X. Sensor Coverage Strategy in Underwater Wireless Sensor Networks. *Int. J. Comput. Commun. Control* **2020**, *15*. https://doi.org/10.15837/ijccc.2020.2.3659.
6. Jiang, P.; Liu, J.; Ruan, B.; et al. A New Node Deployment and Location Dispatch Algorithm for Underwater Sensor Networks. *Sensors* **2016**, *16*, 82. https://doi.org/10.3390/s16010082.
7. Rodríguez García, D.; Montiel-Nelson, J.A.; Bautista, T.; et al. A New Method for Gaining the Control of Standalone Underwater Sensor Nodes Based on Power Supply Sensing. *Sensors* **2021**, *21*, 4660. https://doi.org/10.3390/s21144660.
8. Lloret, J. Underwater Sensor Nodes and Networks. *Sensors* **2013**, *13*, 11782–11796. https://doi.org/10.3390/s130911782.
9. Chang, J.; Shen, X.; Bai, W.; et al. Energy-Efficient Barrier Coverage Based on Nodes Alliance for Intrusion Detection in Underwater Sensor Networks. *IEEE Sens. J.* **2022**, *22*, 3766–3776. https://doi.org/10.1109/JSEN.2021.3140138.
10. Jiang, P.; Liu, J.; Wu, F.; et al. Node Deployment Algorithm for Underwater Sensor Networks Based on Connected Dominating Set. *Sensors* **2016**, *16*, 388. https://doi.org/10.3390/s16030388.
11. Shi, X. Design of a Cylindrical Permanent Magnet Linear Generator for Wave Power Generation. Master's Thesis, Southeast University, Nanjing, China, 2012. (In Chinese)
12. Zhang, Y.; Sheng, S.; You, Y.; et al. Research on Energy Conversion System of Floating Wave Energy Converter. *China Ocean Eng.* **2014**, *28*, 105–113. https://doi.org/10.1007/s13344-014-0008-5.
13. Zou, S.; Robertson, B.; Roach, A.; et al. Wave Energy Converter Arrays: A Methodology to Assess Performance Considering the Disturbed Wave Field. *Renew. Energy* **2024**, *229*, 120719. https://doi.org/10.1016/j.renene.2024.120719.
14. Zhang, D. Design and Experimental Study of a Thermally Driven Underwater Monitoring Platform System. Master's Thesis, Tianjin University, Tianjin, China, 2006. (In Chinese)
15. Liang, Z.; Wang, Y.; Zhang, D.; et al. Study on the Motion Characteristics of a Thermally Driven Vertical-Movement Underwater Monitoring Platform. *J. Sol. Energy* **2016**, *37*, 243–248. (In Chinese)
16. Wang, Y. Performance Analysis and Experimental Study of a Thermally Driven Underwater Monitoring Platform. Master's Thesis, Tianjin University, Tianjin, China, 2004. (In Chinese)
17. Kim, T.H.; Setoguchi, T.; Takao, M.; et al. Study of Turbine with Self-Pitch-Controlled Blades for Wave Energy Conversion. *Int. J. Therm. Sci.* **2002**, *41*, 101–107. https://doi.org/10.1016/S1290-0729(01)01308-4.
18. Zhao, T.; Jiang, Z.; Mo, G.; et al. Control of Separation Flows of Turbine-Blade-Tip Turbines by Splitter Blades. *Proc. Inst. Mech. Eng. A* **2024**, *238*, 985–998. https://doi.org/10.1177/09576509241252877.
19. Zhang, F.; Song, H.; Liu, C.; et al. Study on the Film Cooling Effectiveness of Shaped Holes in the Suction Surface Gill Region of the Turbine Blade. *Int. J. Therm. Sci.* **2023**, *184*, 107977. https://doi.org/10.1016/j.ijthermalsci.2022.107977.
20. Zhang, C.; Fu, X.; Wang, Z. Current Status and Prospects of Triboelectric Nanogenerators in Self-Driven Microsystems Research. *Trans. Chin. Soc. Mech. Eng.* **2019**, *55*, 89–101. (In Chinese)
21. Wang, Z. Commercial Applications of Nanogenerators as Sustainable Power Sources and Active Sensors. *Sci. China Chem.* **2013**, *43*, 759–762. (In Chinese)
22. Yang, K.; Zeng, S.; Yang, K.; et al. From Multi-Field Coupling Behaviors to Self-Powered Monitoring: Triboelectric Nanogenerator Arrays for Deep-Sea Large-Scale Cages. *J. Mar. Sci. Eng.* **2025**, *13*, 2042. https://doi.org/10.3390/jmse13112042.

23. Wang, W.; Chen, G.; Yan, J.; et al. Research on the Power Generation Performance of Solid–Liquid Triboelectric Nanogenerator Based on Surface Microstructure Modification. *Nanomaterials* **2025**, *15*, 872. https://doi.org/10.3390/nano15110872.
24. Wang, W.; Yan, J.; Wang, X.; et al. Research on the Performance of a Liquid–Solid Triboelectric Nanogenerator Prototype Based on Multiphase Liquid. *Micromachines* **2025**, *16*, 78. https://doi.org/10.3390/mi16010078.
25. Wang, Y.; Yang, Y.; Wang, Z.L. Triboelectric Nanogenerators as Flexible Power Sources. *NPJ Flex. Electron.* **2017**, *1*, 10. https://doi.org/10.1038/s41528-017-0007-8.
26. Yang, B.; Li, H.; Wang, Z.; et al. High-Performance Triboelectric Nanogenerator Inspired by Bionic Jellyfish for Wave Energy Harvesting. *Chem. Eng. J.* **2025**, *503*, 158399. https://doi.org/10.1016/j.cej.2024.158399.
27. Gao, Q.; Wang, J.; Li, H.; et al. High Performance Triboelectric Nanogenerator for Wave Energy Harvesting Through the Gas-Assisted Method. *Chem. Eng. J.* **2024**, *493*, 152730. https://doi.org/10.1016/j.cej.2024.152730.
28. Mayer, M.; Xiao, X.; Yin, J.; et al. Advances in Bioinspired Triboelectric Nanogenerators. *Adv. Electron. Mater.* **2022**, *8*, 2200782. https://doi.org/10.1002/aelm.202200782.
29. Li, W.; Pei, Y.; Zhang, C.; et al. Bioinspired Designs and Biomimetic Applications of Triboelectric Nanogenerators. *Nano Energy* **2021**, *84*, 105865. https://doi.org/10.1016/j.nanoen.2021.105865.
30. Zhao, X.J.; Zhu, G.; Zhao, Z.H.; et al. High Durable Bio-Inspired Self-Cleaning Solid-Liquid Contact Triboelectric Nanogenerator for Water Wave Energy Harvesting. *Nano Energy* **2025**, *139*, 110971. https://doi.org/10.1016/j.nanoen.2025.110971.
31. Zhang, Y.; Fu, S.C.; Chan, K.C.; et al. Boosting Power Output of Flutter-Driven Triboelectric Nanogenerator by Flexible Flagpole. *Nano Energy* **2021**, *88*, 106284. https://doi.org/10.1016/j.nanoen.2021.106284.
32. GL RC Certifies Alstom Tidal Turbine Prototype. Marine Technology News 24 April 2013. Available online: https://www.marinetechnologynews.com/news/certifies-alstom-tidal-turbine-476908 (accessed on 24 April 2013).
33. Yuan, P.; Chen, D.; Wang, S.; et al. Experimental Study on Energy Harvesting of Vortex-Induced Vibration Tidal Energy Conversion Device. *J. Ocean Univ. China Nat. Sci. Ed.* **2015**, *45*, 114–120. (In Chinese)
34. Green Power: Stingray Completes First Trial. *Int. Hydropower* **2002**, *6*, 52. (In Chinese)
35. Mutsuda, H.; Tanaka, Y.; Patel, R.; et al. A Painting Type of Flexible Piezoelectric Device for Ocean Energy Harvesting. *Appl. Ocean Res.* **2017**, *68*, 182–193. https://doi.org/10.1016/j.apor.2017.03.009.
36. Cao, L.N.Y.; Xu, Z.; Wang, Z.L. Application of Triboelectric Nanogenerator in Fluid Dynamics Sensing: Past and Future. *Nanomaterials* **2022**, *12*, 3261. https://doi.org/10.3390/nano12193261.
37. Jiang, F.; Zhan, L.; Lee, J.P.; et al. Triboelectric Nanogenerators Based on Fluid Medium: From Fundamental Mechanisms Toward Multifunctional Applications. *Adv. Mater.* **2024**, *36*, 2308197. https://doi.org/10.1002/adma.202308197.
38. Yuan, Z.; Guo, L. Recent Advances in Solid–Liquid Triboelectric Nanogenerator Technologies, Affecting Factors, and Applications. *Sci. Rep.* **2024**, *14*, 10456. https://doi.org/10.1038/s41598-024-60823-y.
39. Zhao, Z.; Wang, X.; Hu, Y.; et al. Investigation on the Tribological Properties and Electrification Performance of Grease-Lubricated Triboelectric Nanogenerators. *Tribol. Int.* **2024**, *191*, 109163. https://doi.org/10.1016/j.triboint.2023.109163.
40. Dong, Y.; Feng, M.; Cheng, J.; et al. Ring-Shaped Single-Electrode Triboelectric Nanogenerator (RSE-TENG) for Energy Harvesting and Liquid Flow Rate Monitoring of Gas-Liquid Two-Phase Flow. *Nano Energy* **2024**, *119*, 109083. https://doi.org/10.1016/j.nanoen.2023.109083.
41. Zhan, T.; Zou, H.; Zhang, H.; et al. Smart Liquid-Piston Based Triboelectric Nanogenerator Sensor for Real-Time Monitoring of Fluid Status. *Nano Energy* **2023**, *111*, 108419. https://doi.org/10.1016/j.nanoen.2023.108419.
42. Li, H.; Zhang, Z.; Xu, P.; et al. A Vortex-Induced Vibration Device Based on MG-TENG and Research of Its Application in Ocean Current Energy Harvesting. *Nano Energy* **2024**, *124*, 109457. https://doi.org/10.1016/j.nanoen.2024.109457.
43. Zhang, L.; Meng, B.; Tian, Y.; et al. Vortex-Induced Vibration Triboelectric Nanogenerator for Low Speed Wind Energy Harvesting. *Nano Energy* **2022**, *95*, 107029. https://doi.org/10.1016/j.nanoen.2022.107029.
44. Wang, Y.; Chen, T.; Sun, S.; et al. A Humidity Resistant and High Performance Triboelectric Nanogenerator Enabled by Vortex-Induced Vibration for Scavenging Wind Energy. *Nano Res.* **2022**, *15*, 3246–3253. https://doi.org/10.1007/s12274-021-3968-9.
45. Wang, Y.; Liu, X.; Chen, T.; et al. An Underwater Flag-Like Triboelectric Nanogenerator for Harvesting Ocean Current Energy Under Extremely Low Velocity Condition. *Nano Energy* **2021**, *90*, 106503. https://doi.org/10.1016/j.nanoen.2021.106503.
46. Shen, C.; Kang, X.; Zhang, R.; et al. The Influence of Vortex Shedding on the Flag Triboelectric Nanogenerators. *Nano Energy* **2025**, *146*, 111564. https://doi.org/10.1016/j.nanoen.2025.111564.
47. Liu, Y.; Wang, P.; Ma, W.; et al. Fish-and Fish-School-Inspired Ocean Current Energy Harvester Array with Triboelectric Nanogenerator. *Device* **2025**, *3*, 100943. https://doi.org/10.1016/j.device.2025.100943.
48. Wei, X.; Zhao, Z.; Zhang, C.; et al. All-Weather Droplet-Based Triboelectric Nanogenerator for Wave Energy Harvesting. *ACS Nano* **2021**, *15*, 13200–13208. https://doi.org/10.1021/acsnano.1c02790.

49. Hutmacher, D.W.; Singh, H. Computational Fluid Dynamics for Improved Bioreactor Design and 3D Culture. *Trends Biotechnol.* **2008**, *26*, 166–172. https://doi.org/10.1016/j.tibtech.2007.11.012.
50. Liu, W.; Wang, Z.; Wang, G.; et al. Integrated Charge Excitation Triboelectric Nanogenerator. *Nat. Commun.* **2019**, *10*, 1426. https://doi.org/10.1038/s41467-019-09464-8.
51. Rodrigues CR, S.; Alves CA, S.; Puga, J.; et al. Triboelectric Driven Turbine to Generate Electricity from the Motion of Water. *Nano Energy* **2016**, *30*, 379–386. https://doi.org/10.1016/j.nanoen.2016.09.038.
52. Xu, W.; Zhou, X.; Hao, C.; et al. SLIPS-TENG: Robust Triboelectric Nanogenerator with Optical and Charge Transparency Using a Slippery Interface. *Natl. Sci. Rev.* **2019**, *6*, 540–550. https://doi.org/10.1093/nsr/nwz025.
53. Ritchie, R.O. The Conflicts Between Strength and Toughness. *Nat. Mater.* **2011**, *10*, 817–822. https://doi.org/10.1038/nmat3115.
54. Shang, W.; Gu, G.Q.; Yang, F.; et al. A Sliding-Mode Triboelectric Nanogenerator with Chemical Group Grated Structure by Shadow Mask Reactive Ion Etching. *ACS Nano* **2017**, *11*, 8796–8803. https://doi.org/10.1021/acsnano.7b02866.
55. Xu, Q.; Shang, C.; Ma, H.; et al. A Guided-Liquid-Based Hybrid Triboelectric Nanogenerator for Omnidirectional and High-Performance Ocean Wave Energy Harvesting. *Nano Energy* **2023**, *109*, 108240. https://doi.org/10.1016/j.nanoen.2023.108240.
56. Sun, X.; Shang, C.; Ma, H.; et al. A Tube-Shaped Solid–Liquid-Interfaced Triboelectric–Electromagnetic Hybrid Nanogenerator for Efficient Ocean Wave Energy Harvesting. *Nano Energy* **2022**, *100*, 107540. https://doi.org/10.1016/j.nanoen.2022.107540.
57. Li, Z.; Zhao, T.; Niu, B.; et al. A Hydrokinetic Turbine-Based Triboelectric-Electromagnetic Hybrid Generator for Ocean Current Energy Harvesting. *Energy Convers. Manag.* **2025**, *326*, 119473. https://doi.org/10.1016/j.enconman.2024.119473.
58. Li, F.; Sun, S.; Wan, X.; et al. A Self-Powered Soft Triboelectric-Electrohydrodynamic Pump. *Nat. Commun.* **2025**, *16*, 1315. https://doi.org/10.1038/s41467-025-56679-z.
59. Zhou, J.; Tao, Y.; Liu, W.; et al. A Portable and Integrated Traveling-Wave Electroosmosis Microfluidic Pumping System Driven by Triboelectric Nanogenerator. *Nano Energy* **2024**, *127*, 109736. https://doi.org/10.1016/j.nanoen.2024.109736.
60. Deng, Z.; Xu, L.; Qin, H.; et al. Rationally Structured Triboelectric Nanogenerator Arrays for Harvesting Water-Current Energy and Self-Powered Sensing. *Adv. Mater.* **2022**, *34*, 2205064. https://doi.org/10.1002/adma.202205064.
61. He, L.; Zhang, C.; Zhang, B.; et al. A Dual-Mode Triboelectric Nanogenerator for Wind Energy Harvesting and Self-Powered Wind Speed Monitoring. *ACS Nano* **2022**, *16*, 6244–6254. https://doi.org/10.1021/acsnano.1c11658.
62. Ni, W.; Jiang, J.; Huang, H.; et al. Research on a Vortex-Induced Vibration Monitoring Sensor Technology Based on Triboelectric Nanogenerator. *Energy* **2025**, *325*, 136121. https://doi.org/10.1016/j.energy.2025.136121.
63. Wang, C.; Guo, H.; Wang, P.; et al. An Advanced Strategy to Enhance TENG Output: Reducing Triboelectric Charge Decay. *Adv. Mater.* **2023**, *35*, 2209895. https://doi.org/10.1002/adma.202209895.
64. Zeng, Q.; Wu, Y.; Tang, Q.; et al. A High-Efficient Breeze Energy Harvester Utilizing a Full-Packaged Triboelectric Nanogenerator Based on Flow-Induced Vibration. *Nano Energy* **2020**, *70*, 104524. https://doi.org/10.1016/j.nanoen.2020.104524.
65. Song, R.; Hou, C.; Yang, C.; et al. Modeling, Validation, and Performance of Two Tandem Cylinder Piezoelectric Energy Harvesters in Water Flow. *Micromachines* **2021**, *12*, 872. https://doi.org/10.3390/mi12080872.
66. Zhu, H.; Tang, T.; Zhou, T.; et al. High Performance Energy Harvesting from Flow-Induced Vibrations in Trapezoidal Oscillators. *Energy* **2021**, *236*, 121484. https://doi.org/10.1016/j.energy.2021.121484.
67. Abdelkefi, A.; Hajj, M.R.; Nayfeh, A.H. Phenomena and Modeling of Piezoelectric Energy Harvesting from Freely Oscillating Cylinders. *Nonlinear Dyn.* **2012**, *70*, 1377–1388. https://doi.org/10.1007/s11071-012-0540-x.
68. Wang, Y.; Liu, X.; Wang, Y.; et al. Research on Underwater Energy Harvesting Technology Based on Flexible Triboelectric Nanogenerators. *J. Underw. Unmanned Syst.* **2022**, *30*, 543–549. (In Chinese)
69. Jiao, P.; Wang, Z.L.; Alavi, A.H. Maximizing Triboelectric Nanogenerators by Physics-Informed AI Inverse Design. *Adv. Mater.* **2024**, *36*, 2308505. https://doi.org/10.1002/adma.202308505.
70. Xie, B.; Guo, Y.; Chen, Y.; et al. Advances in Graphene-Based Electrode for Triboelectric Nanogenerator. *Nano-Micro Lett.* **2025**, *17*, 17. https://doi.org/10.1007/s40820-024-01530-1.
71. Liu, P.B.; Yang, J.; Wei, D.P.; et al. Current Research on Electrode Materials for Flexible Transparent Nanogenerators. *Funct. Mater.* **2017**, *48*, 1019–1028. (In Chinese)
72. Lu, P.; Liao, X.; Guo, X.; et al. Gel-Based Triboelectric Nanogenerators for Flexible Sensing: Principles, Properties, and Applications. *Nano-Micro Lett.* **2024**, *16*, 206. https://doi.org/10.1007/s40820-024-01432-2.
73. Zhang, D.; Shi, J.; Si, Y.; et al. Multi-Grating Triboelectric Nanogenerator for Harvesting Low-Frequency Ocean Wave Energy. *Nano Energy* **2019**, *61*, 132–140. https://doi.org/10.1016/j.nanoen.2019.04.046.
74. Cui, S.; Zhou, L.; Liu, D.; et al. Improving Performance of Triboelectric Nanogenerators by Dielectric Enhancement Effect. *Matter* **2022**, *5*, 180–193. https://doi.org/10.1016/j.matt.2021.10.019.

75. Zhang, S.L.; Xu, M.; Zhang, C.; et al. Rationally Designed Sea Snake Structure Based Triboelectric Nanogenerators for Effectively and Efficiently Harvesting Ocean Wave Energy with Minimized Water Screening Effect. *Nano Energy* **2018**, *48*, 421–429. https://doi.org/10.1016/j.nanoen.2018.03.062.
76. Xiao, Y.; Liu, J.C.; Lv, X.L.; et al. Fabrication of CNT/PDMS Dielectric Layer Microstructures and Friction Nanogenerators. *Trans. Chin. Soc. Mech. Eng.* **2021**, *57*, 177–185. (In Chinese)
77. Guo, Y.B.; Chen, Z.X.; Wang, H.Z.; et al. Research Progress on Triboelectric Nanogenerators Based on Inorganic Filler Composite Films. *J. Inorg. Mater.* **2021**, *36*, 919–928. (In Chinese)
78. Li, S.; Wang, J.; Wang, Z. Recent Advances in Fluid Energy Harvesting Using Triboelectric Nanogenerators. *Acta Mech. Sin.* **2021**, *53*, 2910–2927. (In Chinese)
79. Kang, X.; Pan, C.; Chen, Y.; et al. Boosting Performances of Triboelectric Nanogenerators by Optimizing Dielectric Properties and Thickness of Electrification Layer. *RSC Adv.* **2020**, *10*, 17752–17759. https://doi.org/10.1039/D0RA02181D.
80. Wang, G.; Xi, Y.; Xuan, H.; et al. Hybrid Nanogenerators Based on Triboelectrification of a Dielectric Composite Made of Lead-Free $ZnSnO_3$ Nanocubes. *Nano Energy* **2015**, *18*, 28–36. https://doi.org/10.1016/j.nanoen.2015.09.012.
81. Kim, M.; Park, D.; Alam, M.M.; et al. Remarkable Output Power Density Enhancement of Triboelectric Nanogenerators via Polarized Ferroelectric Polymers and Bulk MoS_2 Composites. *ACS Nano* **2019**, *13*, 4640–4646. https://doi.org/10.1021/acsnano.9b00750.
82. Huang, T.; Yu, H.; Wang, H.; et al. Hydrophobic SiO_2 Electret Enhances the Performance of Poly (Vinylidene Fluoride) Nanofiber-Based Triboelectric Nanogenerator. *J. Phys. Chem. C* **2016**, *120*, 26600–26608. https://doi.org/10.1021/acs.jpcc.6b07382.
83. Mendel, N.; Wu, H.; Mugele, F. Electrowetting-Assisted Generation of Ultrastable High Charge Densities in Composite Silicon Oxide–Fluoropolymer Electret Samples for Electric Nanogenerators. *Adv. Funct. Mater.* **2021**, *31*, 2007872. https://doi.org/10.1002/adfm.202007872.
84. Bo, Z.; Meijia, R.; Wenjian, H.; et al. Study on Temperature-Humidity Controlling Performance of Zeolite-Based Composite and Its Application for Light Quality Energy-Conserving Building Envelope. *Alexandria Eng. J.* **2023**, *69*, 311–321. https://doi.org/10.1016/j.aej.2023.01.032.
85. Li, H.; Guo, Z.; Kuang, S.; et al. Nanocomposite Electret with Surface Potential Self-Recovery from Water Dipping for Environmentally Stable Energy Harvesting. *Nano Energy* **2019**, *64*, 103913. https://doi.org/10.1016/j.nanoen.2019.103913.
86. Bhagat, N.; Saxena, V.; Singh, A.; et al. Fabrication of Solution Processable Perovskite Solar Cells Under High Humid Conditions via Optimization of TiO_2 Compact Layer. *Int. J. Mod. Phys. B* **2024**, *38*, 2450250. https://doi.org/10.1142/S0217979224502503.
87. Wang, D.; Zhang, D.; Tang, M.; et al. Ethylene Chlorotrifluoroethylene/Hydrogel-Based Liquid-Solid Triboelectric Nanogenerator Driven Self-Powered MXene-Based Sensor System for Marine Environmental Monitoring. *Nano Energy* **2022**, *100*, 107509. https://doi.org/10.1016/j.nanoen.2022.107509.
88. Zhang, M.; Xia, L.; Dang, S.; et al. A Flexible Single-Electrode-Based Triboelectric Nanogenerator Based on Double-Sided Nanostructures. *AIP Adv.* **2019**, *9*, 075221. https://doi.org/10.1063/1.5114884.
89. Dan, H.; Li, H.; Yang, Y. Flexible Ferroelectric Materials-Based Triboelectric Nanogenerators for Mechanical Energy Harvesting. *Front. Mater.* **2022**, *9*, 939173. https://doi.org/10.3389/fmats.2022.939173.
90. Rocha-Ortiz, G.; Gonzalez-Gutierrez, A.G.; Casillas-Santana, N.; et al. Innovative Dielectric Polyaniline Composites for Performance Triboelectric Nanogenerators. *J. Solid State Electrochem.* **2025**, *29*, 3237–3251. https://doi.org/10.1007/s10008-024-06122-y.
91. Li, Y.; Luo, Y.; Deng, H.; et al. Advanced Dielectric Materials for Triboelectric Nanogenerators: Principles, Methods, and Applications. *Adv. Mater.* **2024**, *36*, 2314380. https://doi.org/10.1002/adma.202314380.
92. Zhao, Z.; Zhou, L.; Li, S.; et al. Selection Rules of Triboelectric Materials for Direct-Current Triboelectric Nanogenerator. *Nat. Commun.* **2021**, *12*, 4686. https://doi.org/10.1038/s41467-021-25046-z.
93. Moradi, F.; Karimzadeh, F.; Kharaziha, M. Rational Micro/Nano-Structuring for High-Performance Triboelectric Nanogenerator. *J. Alloys Compd.* **2023**, *960*, 170693. https://doi.org/10.1016/j.jallcom.2023.170693.
94. Feng, L.; Wu, Y.; Qu, J.; et al. Advancing Liquid-Solid Triboelectric Nanogenerators via Micro/Nano-Structured Interface Engineering. *Compos. B Eng.* **2025**, *309*, 113081. https://doi.org/10.1016/j.compositesb.2025.113081.
95. Zhang, B.; Shen, A.; Jing, Y.; et al. Flexible Nanostructured Polymer Materials Based Triboelectric Nanogenerators for Self-Powered Environmental Sensing. *Small Methods* **2025**, *9*, e01241. https://doi.org/10.1002/smtd.202501241.
96. Tcho, I.W.; Kim, W.G.; Jeon, S.B.; et al. Surface Structural Analysis of a Friction Layer for a Triboelectric Nanogenerator. *Nano Energy* **2017**, *42*, 34–42. https://doi.org/10.1016/j.nanoen.2017.10.037.
97. Ru, C.; Yin, J.; Xu, L. Biomimetic Strawberry-Structured Micro/Nano Fibers as Positive Friction Layers for High-Performance Triboelectric Nanogenerators. *Biomacromolecules* **2025**, *26*, 7097–7107. https://doi.org/10.1021/acs.biomac.5c01403.

98. Zhao, L.; Zheng, Q.; Ouyang, H.; et al. A Size-Unlimited Surface Microstructure Modification Method for Achieving High Performance Triboelectric Nanogenerator. *Nano Energy* **2016**, *28*, 172–178. https://doi.org/10.1016/j.nanoen.2016.08.024.
99. Zhao, L.; Su, W.; Yang, X.; et al. Effect of Interface Microstructures on the Performance of Droplet-Based Triboelectric Nanogenerator. *Energy Mater. Adv*. **2026**, *1*, 0231. https://doi.org/10.34133/energymatadv.0231.
100. Chen, H.; Wang, J.; Ning, A. Optimization of a Rolling Triboelectric Nanogenerator Based on the Nano–Micro Structure for Ocean Environmental Monitoring. *ACS Omega* **2021**, *6*, 21059–21065. https://doi.org/10.1021/acsomega.1c02709.
101. Gokhool, S.; Bairagi, S.; Kumar, C.; et al. Reflections on Boosting Wearable Triboelectric Nanogenerator Performance via Interface Optimisation. *Results Eng.* **2023**, *17*, 100808. https://doi.org/10.1016/j.rineng.2022.100808.
102. Lin, Z.-H.; Kim, S.-J.; Wang, Z.; et al. Advancements in Solid–Liquid Triboelectric Nanogenerators. *MRS Bull.* **2025**, *50*, 491–502. https://doi.org/10.1557/s43577-025-00868-0.
103. Zhang, J.; Wu, C.; Mo, X.; et al. Triboelectric Nanogenerators as a Probe for Studying Charge Transfer at Liquid–Solid Interface. *MRS Bull.* **2025**, *50*, 327–335. https://doi.org/10.1557/s43577-024-00847-x.
104. Xiang, T.; Chen, X.; Sun, H.; et al. Advances in Liquid-Solid Triboelectric Nanogenerators and Its Applications. *J. Mater. Sci. Technol.* **2025**, *214*, 153–169. https://doi.org/10.1016/j.jmst.2024.07.013.
105. Wang, K.; Wang, X.; Sun, Y.; et al. Macroscopic Liquid Superlubric Triboelectric Nanogenerator: An In-Depth Understanding of Solid-Liquid Interfacial Charge Behavior. *Nano Energy* **2024**, *129*, 110038. https://doi.org/10.1016/j.nanoen.2024.110038.
106. Li, X.; Zhang, D.; Zhang, D.; et al. Solid-Liquid Triboelectric Nanogenerator Based on Vortex-Induced Resonance. *Nanomaterials* **2023**, *13*, 1036. https://doi.org/10.3390/nano13061036.
107. Chen, P.; Zhang, Z.; Ye, C.; et al. A Self-Sustainable, Ultrarobust and High-Power-Density Triboelectric Nanogenerator for In Situ Powering of Marine Internet of Things. *Adv. Mater.* **2025**, *37*, e11283. https://doi.org/10.1002/adma.202511283.
108. Wang, Y.; Liu, X.; Wang, Y.; et al. Flexible Seaweed-Like Triboelectric Nanogenerator as a Wave Energy Harvester Powering Marine Internet of Things. *ACS Nano* **2021**, *15*, 15700–15709. https://doi.org/10.1021/acsnano.1c05127.
109. Gai, Y.; Jin, B.; Wang, E.; et al. Adaptive Dual Turbine Triboelectric Nanogenerator Toward Self-Powered Marine Buoy. *Nano Energy* **2025**, *144*, 111356. https://doi.org/10.1016/j.nanoen.2025.111356.
110. Triboelectric Nanogenerators (Adv. Funct. Mater. 41/2019). *Adv. Funct. Mater.* **2019**, *29*, 1970287. https://doi.org/10.1002/adfm.201970287.
111. Gao, L.; Xu, X.; Han, H.; et al. A Broadband Hybrid Blue Energy Nanogenerator for Smart Ocean IoT Network. *Nano Energy* **2024**, *127*, 109697. https://doi.org/10.1016/j.nanoen.2024.109697.
112. Wang, Z.L.; Jiang, T.; Xu, L. Toward the Blue Energy Dream by Triboelectric Nanogenerator Networks. *Nano Energy* **2017**, *39*, 9–23. https://doi.org/10.1016/j.nanoen.2017.06.035.
113. Hao, Y.; Wu, C.; Zang, K.; et al. Research Advances of Triboelectric Nanogenerators for Blue Energy: Research Status, Challenges and Future Outlook. *Nano Energy* **2025**, *142*, 111223. https://doi.org/10.1016/j.nanoen.2025.111223.
114. Li, H.; Wang, J.; Liang, L.; et al. Design of an Efficient Blue Energy Harvesting System Based on Triboelectric Nanogenerators with Frequency Upconversion and Networking Strategies. *Nano Energy* **2025**, *140*, 110993. https://doi.org/10.1016/j.nanoen.2025.110993.
115. He, J.; Wang, X.; Nan, Y.; et al. Research Progress of Triboelectric Nanogenerators for Ocean Wave Energy Harvesting. *Small* **2025**, *21*, 2411074. https://doi.org/10.1002/smll.202411074.
116. Wang, W.; Yang, D.; Yan, X.; et al. Triboelectric Nanogenerators: The Beginning of Blue Dream. *Front. Chem. Sci. Eng.* **2023**, *17*, 635–678. https://doi.org/10.1007/s11705-022-2271-y.
117. Cheng, T.; Shao, J.; Wang, Z.L. Triboelectric Nanogenerators. *Nat. Rev. Methods Primers* **2023**, *3*, 39. https://doi.org/10.1038/s43586-023-00220-3.
118. Shao, J.; Yang, Y.; Yang, O.; et al. Designing Rules and Optimization of Triboelectric Nanogenerator Arrays. *Adv. Energy Mater.* **2021**, *11*, 2100065. https://doi.org/10.1002/aenm.202100065.
119. Chen, Z.; Ye, R.; Lee, W.; et al. Magnetization-Induced Self-Assembling of Bendable Microneedle Arrays for Triboelectric Nanogenerators. *Adv. Electron. Mater.* **2019**, *5*, 1800785. https://doi.org/10.1002/aelm.201800785.
120. Liu, W.; Xu, L.; Bu, T.; et al. Torus Structured Triboelectric Nanogenerator Array for Water Wave Energy Harvesting. *Nano Energy* **2019**, *58*, 499–507. https://doi.org/10.1016/j.nanoen.2019.01.088.
121. Lv, S.; Zhang, X.; Huang, T.; et al. Interconnected Array Design for Enhancing the Performance of an Enclosed Flexible Triboelectric Nanogenerator. *Nano Energy* **2021**, *89*, 106476. https://doi.org/10.1016/j.nanoen.2021.106476.
122. Sun, Z.; Yang, W.; Chen, P.; et al. Effects of PDMS Base/Agent Ratios and Texture Sizes on the Electrical Performance of Triboelectric Nanogenerators. *Adv. Mater. Interfaces* **2022**, *9*, 2102139. https://doi.org/10.1002/admi.202102139.
123. Zou, Y.; Xu, J.; Chen, K.; et al. Triboelectric Nanogenerators: Advances in Nanostructures for High-Performance Triboelectric Nanogenerators. *Adv. Mater. Technol.* **2021**, *6*, 2170016. https://doi.org/10.1002/admt.202170016.
124. Zhao, D.; Yu, X.; Wang, Z.; et al. Universal Equivalent Circuit Model and Verification of Current Source for Triboelectric Nanogenerator. *Nano Energy* **2021**, *89*, 106335. https://doi.org/10.1016/j.nanoen.2021.106335.

125. Cha, K.; In, S.; Chung, S.H.; et al. Improving Electrical Performance and Lifespan of Liquid-Based Triboelectric Nanogenerator via Charge-Inducing Structure. *Adv. Funct. Mater.* **2025**, *35*, 2505695. https://doi.org/10.1002/adfm.202505695.
126. Kim, W.G.; Kim, D.W.; Tcho, I.W.; et al. Triboelectric Nanogenerator: Structure, Mechanism, and Applications. *ACS Nano* **2021**, *15*, 258–287. https://doi.org/10.1021/acsnano.0c09803.
127. Liu, W.; Xu, L.; Liu, G.; et al. Network Topology Optimization of Triboelectric Nanogenerators for Effectively Harvesting Ocean Wave Energy. *iScience* **2020**, *23*, 101848. https://doi.org/10.1016/j.isci.2020.101848.
128. Liu, W.; Xu, L.; Liu, G.; et al. Output Characteristics of Series-Parallel Triboelectric Nanogenerators. *Nanotechnology* **2023**, *34*, 155403. https://doi.org/10.1088/1361-6528/aca599.
129. Liang, X.; Liu, S.; Yang, H.; et al. Triboelectric Nanogenerators for Ocean Wave Energy Harvesting: Unit Integration and Network Construction. *Electronics* **2023**, *12*, 225. https://doi.org/10.3390/electronics12010225.
130. Liang, X.; Jiang, T.; Liu, G.; et al. Triboelectric Nanogenerator Networks Integrated with Power Management Module for Water Wave Energy Harvesting. *Adv. Funct. Mater.* **2019**, *29*, 1807241. https://doi.org/10.1002/adfm.201807241.
131. Xie, L.; Zhai, N.; Liu, Y.; et al. Hybrid Triboelectric Nanogenerators: From Energy Complementation to Integration. *Research* **2021**, *2021*, 9143762. https://doi.org/10.34133/2021/9143762.
132. Ahmed, A.; Hassan, I.; El-Kady, M.F.; et al. Integrated Triboelectric Nanogenerators in the Era of the Internet of Things. *Adv. Sci.* **2019**, *6*, 1802230. https://doi.org/10.1002/advs.201802230.
133. Wang, J.; Zhang, H.; Xie, Y.; et al. Smart Network Node Based on Hybrid Nanogenerator for Self-Powered Multifunctional Sensing. *Nano Energy* **2017**, *33*, 418–426. https://doi.org/10.1016/j.nanoen.2017.01.055.
134. Li, H.; Liang, C.; Ning, H.; et al. O-ring-Modularized Triboelectric Nanogenerator for Robust Blue Energy Harvesting in All-Sea Areas. *Nano Energy* **2022**, *103*, 107812. https://doi.org/10.1016/j.nanoen.2022.107812.
135. Harmon, W.; Bamgboje, D.; Guo, H.; et al. Self-Driven Power Management System for Triboelectric Nanogenerators. *Nano Energy* **2020**, *71*, 104642. https://doi.org/10.1016/j.nanoen.2020.104642.
136. Qin, H.; Gu, G.; Shang, W.; et al. A Universal and Passive Power Management Circuit with High Efficiency for Pulsed Triboelectric Nanogenerator. *Nano Energy* **2020**, *68*, 104372. https://doi.org/10.1016/j.nanoen.2019.104372.
137. Xi, F.; Pang, Y.; Li, W.; et al. Universal Power Management Strategy for Triboelectric Nanogenerator. *Nano Energy* **2017**, *37*, 168–176. https://doi.org/10.1016/j.nanoen.2017.05.027.
138. Cheng, X.; Miao, L.; Song, Y.; et al. High Efficiency Power Management and Charge Boosting Strategy for a Triboelectric Nanogenerator. *Nano Energy* **2017**, *38*, 438–446. https://doi.org/10.1016/j.nanoen.2017.05.063.
139. Zi, Y.; Guo, H.; Wang, J.; et al. An Inductor-Free Auto-Power-Management Design Built-in Triboelectric Nanogenerators. *Nano Energy* **2017**, *31*, 302–310. https://doi.org/10.1016/j.nanoen.2017.05.025.
140. Niu, S.; Zhou, Y.S.; Wang, S.; et al. Simulation Method for Optimizing the Performance of an Integrated Triboelectric Nanogenerator Energy Harvesting System. *Nano Energy* **2014**, *8*, 150–156. https://doi.org/10.1016/j.nanoen.2014.05.018.
141. Liang, X.; Jiang, T.; Feng, Y.; et al. Triboelectric Nanogenerator Network Integrated with Charge Excitation Circuit for Effective Water Wave Energy Harvesting. *Adv. Energy Mater.* **2020**, *10*, 2002123. https://doi.org/10.1002/aenm.202002123.
142. Liu, L.; Guo, X.; Lee, C. Promoting Smart Cities into the 5G Era with Multi-Field Internet of Things (IoT) Applications Powered with Advanced Mechanical Energy Harvesters. *Nano Energy* **2021**, *88*, 106304. https://doi.org/10.1016/j.nanoen.2021.106304.
143. Delgado-Alvarado, E.; Morales-Gonzalez, E.A.; Gonzalez-Calderon, J.A.; et al. Recent Advances of Hybrid Nanogenerators for Sustainable Ocean Energy Harvesting: Performance, Applications, and Challenges. *Technologies* **2025**, *13*, 336. https://doi.org/10.3390/technologies13080336.
144. Liu, Y.; Hu, C. Triboelectric Nanogenerators Based on Elastic Electrodes. *Nanoscale* **2020**, *12*, 20118–20130. https://doi.org/10.1039/D0NR04868B.
145. Liu, L.; Shi, Q.; Ho, J.S.; et al. Study of Thin Film Blue Energy Harvester Based on Triboelectric Nanogenerator and Seashore IoT Applications. *Nano Energy* **2019**, *66*, 104167. https://doi.org/10.1016/j.nanoen.2019.104167.
146. Ye, Z.; Liu, S.; Wang, W.; et al. Full-Response Triboelectric Nanogenerator Modeling and Sensing Framework: Zero State and Zero Input in Synergy. *Device* **2025**, *3*, 100872. https://doi.org/10.1016/j.device.2025.100872.
147. Song, Y.; Wang, N.; Wang, Y.; et al. Direct Current Triboelectric Nanogenerators. *Adv. Energy Mater.* **2020**, *10*, 2002756. https://doi.org/10.1002/aenm.202002756.
148. Wu, C.; Huang, H.; Li, R.; et al. Research on the Potential of Spherical Triboelectric Nanogenerator for Collecting Vibration Energy and Measuring Vibration. *Sensors* **2020**, *20*, 1063. https://doi.org/10.3390/s20041063.
149. Zhang, S.; Shi, Z.; Yuan, X.; et al. Fish Schooling Effect Triboelectric Nanogenerators Array. *Nano Energy* **2025**, *142*, 111263. https://doi.org/10.1016/j.nanoen.2025.111263.
150. Kaur, N.; Pal, K. Triboelectric Nanogenerators for Mechanical Energy Harvesting. *Energy Technol.* **2018**, *6*, 958–997. https://doi.org/10.1002/ente.201700639.

151. Zhang, H.; Li, Y.; Jiang, W.; et al. Marine Environment Numerical Simulation of Morphological Planning of Land Reclamation. *Proc. Inst. Mech. Eng. M* **2022**, *236*, 996–1011. https://doi.org/10.1177/14750902221079478.
152. Rusu, E.; Măcuță, S. Numerical Modelling of Longshore Currents in Marine Environment. *Environ. Eng. Manag. J.* **2009**, *8*, 147–151. https://doi.org/10.30638/eemj.2009.022.
153. Ji, J.; Zhou, L.; Liu, B.; et al. Experimental and Numerical Analysis of a Bottom-Supported Aquaculture Platform in Uniform Flow. *Ocean Eng.* **2024**, *311*, 118859. https://doi.org/10.1016/j.oceaneng.2024.118859.
154. Nejad, J.V.N.; Kheradmand, S. The Effect of Fluctuating Boundary on Flow Field and Performance Parameters of Cyclone Separator. *Powder Technol.* **2021**, *390*, 401–416. https://doi.org/10.1016/j.powtec.2021.05.055.
155. Tan, P.; Sha, Y.; Bai, X.; et al. A Performance Test and Internal Flow Field Simulation of a Vortex Pump. *Appl. Sci.* **2017**, *7*, 1273. https://doi.org/10.3390/app7121273.
156. Yang, C.; Lu, Z.; Hao, Z.; et al. Numerical Simulation and Design Optimization of a Circulating Water Channel on Hydrodynamic Flow Performance. *J. Mar. Sci. Technol.* **2024**, *29*, 493–507. https://doi.org/10.1007/s00773-024-01003-5.
157. Gucheng, Z.; Zuogang, C.; Yi, D. A Numerical Investigation on Hydrodynamic Characteristics of the Circulating Water Channel. *Ocean Eng.* **2021**, *236*, 109564. https://doi.org/10.1016/j.oceaneng.2021.109564.
158. Zhang, L.; Shan, X.; Xie, T. Enhancing Flow Field Performance of a Small Circulating Water Channel Based on Porous Grid Plate. *Appl. Sci.* **2020**, *10*, 5103. https://doi.org/10.3390/app10155103.
159. Liu, H.; Zhou, Y.; Ren, X.; et al. Numerical Modeling and Application of the Effects of Fish Movement on Flow Field in Recirculating Aquaculture System. *Ocean Eng.* **2023**, *285*, 115432. https://doi.org/10.1016/j.oceaneng.2023.115432.
160. Jaeger, A.; Coll, C.; Posselt, M.; et al. Using Recirculating Flumes and a Response Surface Model to Investigate the Role of Hyporheic Exchange and Bacterial Diversity on Micropollutant Half-Lives. *Environ. Sci. Process. Impacts* **2019**, *21*, 2093–2108. https://doi.org/10.1039/C9EM00327D.
161. Ni, W.; Tian, G.; Yang, C.; et al. Simultaneous Energy Utilization and Vibration Suppression Study of a Rolling-Structured Triboelectric Nanogenerator for the Vortex-Induced Vibration of a Cylinder. *Ocean Eng.* **2023**, *288*, 115976. https://doi.org/10.1016/j.oceaneng.2023.115976.
162. Zhang, S.; Jing, Z.; Wang, X.; et al. Soft-Bionic-Fishtail Structured Triboelectric Nanogenerator Driven by Flow-Induced Vibration for Low-Velocity Water Flow Energy Harvesting. *Nano Res.* **2023**, *16*, 466–472. https://doi.org/10.1007/s12274-022-4715-6.
163. Kim, H.; Zhou, Q.; Kim, D.; et al. Flow-Induced Snap-Through Triboelectric Nanogenerator. *Nano Energy* **2020**, *68*, 104379. https://doi.org/10.1016/j.nanoen.2019.104379.
164. Ahmed, A. Self-Powered Wireless Sensing Platform for Monitoring Marine Life Based on Harvesting Hydrokinetic Energy of Water Currents. *J. Mater. Chem. A* **2022**, *10*, 1992–1998. https://doi.org/10.1039/D1TA04861A.
165. Han, J.; Shui, Y.; Nie, L.; et al. Unsteady Flow Control Mechanisms of a Bio-Inspired Flexible Flap with the Fluid–Structure Interaction. *Phys. Fluids* **2023**, *35*. https://doi.org/10.1063/5.0145805.
166. Chao, T.; Can, S.; Li-bo, Q.I.; et al. Theory and Applications of Coupled Fluid-Structure Interactions of Ships in Waves and Ocean Acoustic Environment. *J. Hydrodyn.* **2016**, *28*, 923–936. https://doi.org/10.1016/S1001-6058(16)60694-7.
167. Huang, Y.; Xiao, Q.; Idarraga, G.; et al. Bio-Inspired Adaptive Flexible Tube Wave Energy Converters: Resonant Fluid–Structure Interaction and Power Extraction. *Phys. Fluids* **2025**, *37*, 0531104. https://doi.org/10.1063/5.0270834.
168. Yu, G.; Wen, J.; Li, H.; et al. Vibration-Coupled TENGs from Weak to Ultra-Strong Induced by Vortex for Harvesting Low-Grade Airflow Energy. *Nano Energy* **2024**, *119*, 109062. https://doi.org/10.1016/j.nanoen.2023.109062.
169. Ren, Z.; Wang, Z.; Liu, Z.; et al. Energy Harvesting from Breeze Wind (0.7–6 m s^{-1}) Using Ultra-Stretchable Triboelectric Nanogenerator. *Adv. Energy Mater.* **2020**, *10*, 2001770. https://doi.org/10.1002/aenm.202001770.
170. Leclercq, T.; de Langre, E. Vortex-Induced Vibrations of Cylinders Bent by the Flow. *J. Fluids Struct.* **2018**, *80*, 77–93. https://doi.org/10.1016/j.jfluidstructs.2018.03.008.
171. Kwak, S.S.; Kim, S.M.; Ryu, H.; et al. Butylated Melamine Formaldehyde as a Durable and Highly Positive Friction Layer for Stable, High Output Triboelectric Nanogenerators. *Energy Environ. Sci.* **2019**, *12*, 3156–3163. https://doi.org/10.1039/c9ee01267b.
172. Wang, J.; Geng, L.; Ding, L.; et al. The State-of-the-Art Review on Energy Harvesting from Flow-Induced Vibrations. *Appl. Energy* **2020**, *267*, 114902. https://doi.org/10.1016/j.apenergy.2020.114902.
173. Li, H.; Wen, J.; Ou, Z.; et al. Leaf-Like TENGs for Harvesting Gentle Wind Energy at An Air Velocity as Low as 0.2 m s^{-1}. *Adv. Funct. Mater.* **2023**, *33*, 2212207. https://doi.org/10.1002/adfm.202212207.
174. Jiang, Y.; Liang, X.; Jiang, T.; et al. Advances in Triboelectric Nanogenerators for Blue Energy Harvesting and Marine Environmental Monitoring. *Engineering* **2024**, *33*, 204–224. https://doi.org/10.1016/j.eng.2023.05.023.
175. Wu, Y.; Wang, X.; Yang, L.; et al. Pressurized Well-Inspired Triboelectric Nanogenerators for Harvesting Water Wave Energy Toward Marine Environmental Applications. *J. Mater. Chem. A* **2025**, *13*, 27125–27135. https://doi.org/10.1039/D4TA09110H.

176. Shankaregowda, S.A.; Nanjegowda, C.B.; Guan, S.; et al. A Robust Triboelectric Nanogenerator Resistant to Humidity and Temperature in Ambient Environment. *Phys. Status Solidi RRL* **2023**, *17*, 2200489. https://doi.org/10.1002/pssr.202200489.
177. Wu, M.; Guo, W.; Dong, S.; et al. A Hybrid Triboelectric Nanogenerator for Enhancing Corrosion Prevention of Metal in Marine Environment. *NPJ Mater. Degrad.* **2022**, *6*, 73. https://doi.org/10.1038/s41529-022-00272-y.
178. Somkuwar, V.U.; Garg, H.; Maurya, S.K.; et al. Influence of Relative Humidity and Temperature on the Performance of Knitted Textile Triboelectric Nanogenerator. *ACS Appl. Electron. Mater.* **2024**, *6*, 931–939. https://doi.org/10.1021/acsaelm.3c01442.